JAMES COOK CYCLONE STRUCTURAL TESTING STATION

CYCLONE TESTING STATION

BEHAVIOUR OF DIFFERENT PROFILED ROOFING SHEETS SUBJECT TO WIND UPLIFT

TECHNICAL REPORT No. 37

October 1992

CYCLONE TESTING STATION

BEHAVIOUR OF DIFFERENT PROFILED ROOFING SHEETS SUBJECT TO WIND UPLIFT

Y.L. Xu

G.F. Reardon

TECHNICAL REPORT No. 37

Xu, Y.L. (You Lin), 1952- .
Behaviour of different profiled roofing sheets subject to wind uplift.

ISBN 0 86443 456 1.
ISSN 0158 - 8338

1. Roofs - Aerodynamics. 2. Roofing, Iron and steel - Testing. 3. Sheet-metal. 4. Building, Stormproof. I. Reardon, G. F. (Gregory Frederick), 1937- . II. James Cook University of North Queensland. Cyclone Testing Station. III. Title. (Series: Technical Report (James Cook University of North Queensland. Cyclone Testing Station); no 37).

690.15

BEHAVIOUR OF DIFFERENT PROFILED ROOFING SHEETS SUBJECT TO WIND UPLIFT

Synopsis

A series of static tests was performed on three types of light gauge steel roofing sheets to investigate effects of sheeting profiles on roofing structural behaviour under simulated wind uplift. The considered sheeting profiles were arc-tangent, trapezoidal and ribbed, and an alternate (or equivalent alternate) sheeting crest fastening system was adopted. Different roofing spans and sheeting thicknesses were included in the tests, and the effect of cyclone washers on static performance of the roofing sheets was estimated. The experimental results show that the roof sheeting behaviour under wind uplift was greatly dependent on the sheeting profiles. The shape and height of screw fastened crests affected limit values of initial failure or ultimate strength of the roofing sheets. The use of cyclone washers reduced local plastic deformation around the screw fasteners at the central support and, in general, increased the slope of load-deflection curves and failure strength. Increasing of roofing span slightly reduced the limit values of reaction force per fastener, but the allowable wind pressure still should be decreased. The use of thicker roofing sheets enhanced the roofing static failure strength and sometimes changed the roofing failure modes.

The midspan load method which has been used in roof sheeting tests was also examined in this project. The measured load-fastener reaction force curves showed that two-span continuous simply supported beam assumption was reasonable in most cases. However, during large cross-sectional distortion or large local plastic deformation, such assumption was not satisfactory. The experimental results obtained by using two types of midspan loading pads indicated that the effect of loading pad surface on initial failure strength of the roofing sheets was considerable.

CONTENTS

1 INTRODUCTION

Profiled steel sheets play an important role in light gauge metal building construction, particularly as a roof cladding in houses, low rise commercial and industrial buildings. Numerous types of cold-formed roofing sheets with different profiles and coatings have been now produced by many manufacturers throughout the world. Such high tensile steel profiled roofing sheets are usually screw-fastened to cold-formed steel purlins or high quality timber purlins to construct very common roof systems. When used in wind prone area, structural performance of such roof systems under wind loads becomes a main criterion for structural design engineers. However, limited information on the structural behaviour of roof systems under wind loads is available in the public domain.

Wind pressures acting on roofs are actually fluctuating, large in amplitude and rapid with time. The fluctuations in pressure are due to two separate but interacting flow phenomena - firstly the natural turbulence or gustiness in the wind, and secondly the local pressure fluctuations at sharp corners and roof-wall junctions where the flow separates from the surface, and vortices and eddies are formed. Since the inertial effect of light gauge steel roofing under fluctuating wind loads is negligible, structural behaviour of roof systems in which designers are concerned is usually static or fatigue. In this report, only the static behaviour of different profiled roofing sheets is discussed.

Parsons (1976) conducted an extensive tests of steel claddings under static and cyclic wind loads for commercial purposes. Only the maximum allowable wind load which the cladding can sustain without permanent deformation was involved in the static wind load tests. Beck and Stevens (1976, 1979), and Morgan and Beck (1977) probably first performed the fatigue test of arc-tangent type roofing sheets. Before the fatigue tests, some static tests simulating wind uplift were carried out by them on the roofing sheets with an alternate crest fastening arrangement. They found that a local diamond-shape deformation progressively developed in the crest of the corrugation under the head of the screw fasteners, which was followed by an elastic buckle at a nominal fastener reaction force of 700 Newtons per fastener. Mahendran (1990) investigated the static behaviour of arc-tangent type roofing sheets under simulated wind uplift in detail, considering the effects of cyclone washers, roofing spans and fastener spacings on roof sheeting properties. It was found that for a roofing assembly with alternate crest fastening systems, the local plastic buckling "load", in terms of average

fastener reaction force, was independent on roofing spans and could be significantly increased by using cyclone washers.

In this investigation, three types of two-span roofing sheets were tested under simulated wind uplift to enhance the understanding of structural behaviour of roofing assemblies and the recognition of the importance of roof sheeting geometric profiles. The sheeting profiles concerned here were arc-tangent, trapezoidal and ribbed. The effects of cyclone washers, roofing spans and sheeting thicknesses on structural behaviour of roofing assemblies were estimated in terms of roof sheeting deflection and initial or ultimate failure load. The modelling requirement of prototype roofing assembly in the test was discussed, based on loading pads, measured load-fastener reaction curves. The obtained test results also provide a basis for a finite element analysis and fatigue tests of the corresponding roofing assemblies in the consequent research work.

2. EXPERIMENTAL ARRANGEMENT

2.1 Sheeting Types and Screw Fastenings

The basic types of roofing sheets used in this research were Lysaght regular CUSTOM ORB, SPANDEK and TRIMDEK sheetings of 0.47 mm nominal thickness including coatings. The roofing sheets are roll-formed from Zincalume-coated high tensile steel sheets. In this report, their profiles were classified as arc-tangent, trapezoidal and ribbed types, respectively. Lysaght heavy SPANDEK sheeting of 0.53 mm total coated thickness and Lysaght regular CUSTOM BLUE ORB sheeting of 0.66 mm total coated thickness were occasionally used. The profiles and basic dimensions of the roofing sheets are shown in Fig. 2.1 (after Lysaght, 1990).

When timber purlins are chosen as the support of roofing sheets, alternate crest fastening with or without cyclone washers is often recommended for end supports and end laps with regard to arc-tangent and trapezoidal type sheets by the manufacturers of the roofing sheets (Lysaght, 1990). For ribbed type sheets, every crest fastening system is recommended for both end and internal supports due to wide pans. Type 17 self-drilling wood screws with hexagonal head and EPDM seal shown in Fig. 2.2(a) are used to secure the roofing sheets to timber battens (Lysaght, 1991). The additional cyclone washers are shown in Fig. 2.2(b) for arc-tangent type sheet and in Fig. 2.2(c) for trapezoidal and ribbed type sheet.

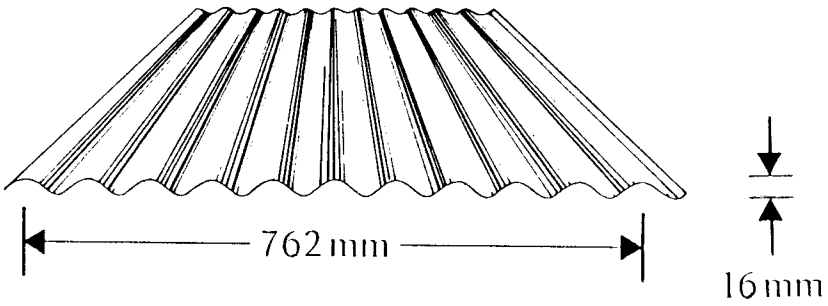

(a) Arc-Tangent Type

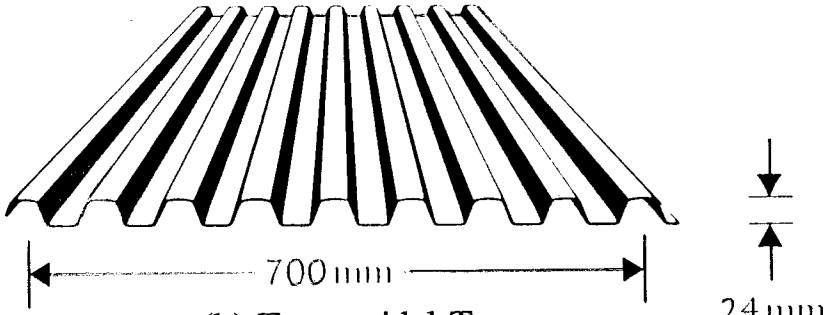

(b) Trapezoidal Type

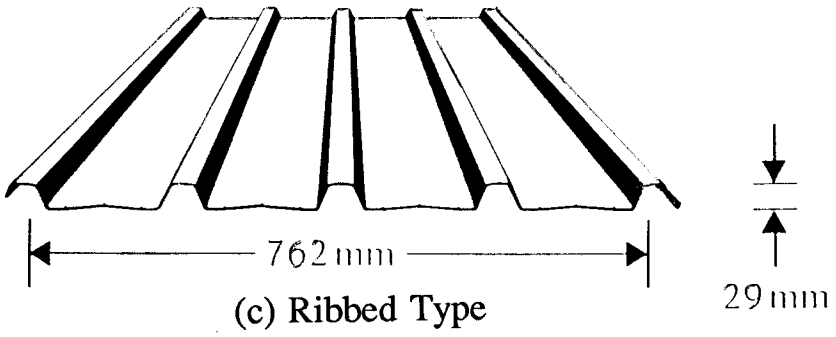

(c) Ribbed Type

FIG. 2.1 SHEETING PROFILES USED IN TESTS

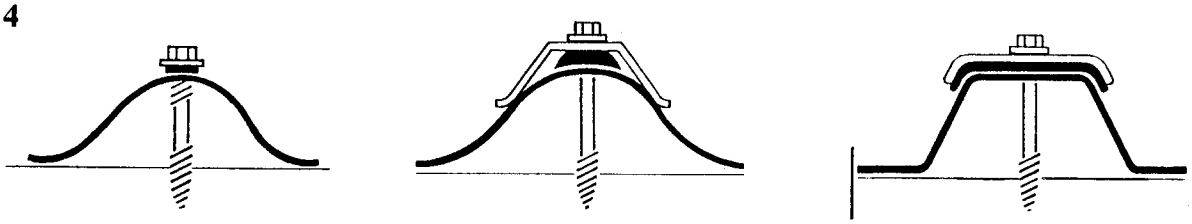

(a)
Screw Fastener

(b)
Screw Fastener with Cyclone Washer for Custom Orb

(c)
Screw Fastener with Cyclone Washer for Spandek and Trimdek

FIG.2.2 SCREW FASTENER AND CYCLONE WASHERS

2.2 Modelling of Prototype Roof Assembly

Aerodynamic loads acting on the roof and wall of a low building are determined by the interaction of wind flow with the surface of the building. From a large quantity of wind tunnel tests and field measurements, it is found that the roof claddings are predominantly subjected to wind suction, i.e., wind uplift, and very high suction is developed at the roof eaves close to the roof corner. Therefore, a multi-span assembly of roof-cladding prototype can be conservatively approximated by a model consisting of a two-span roofing assembly subjected to uniformly-distributed uplift loading (Beck and Stevens, 1979). The critical second support from the eaves of the roof prototype can be represented by the central support of the two-span roof model.

There are currently three methods being used to test roof sheeting, that is, vacuum chamber method, air bag method and midspan load method. In the vacuum chamber method, one surface of the roof sheeting is fitted in the chamber and sealed with some plastic sheeting. The air is sucked from the chamber and the wind suction acting on the sheeting is simulated (Gerhardt and Kramer, 1986; Hancock, 1991). In the air bag method, special bags pumped with air contact with the roof sheeting surface directly to develop a distributed loading. As for the midspan load method, midspan line loads across the full width of the sheet are used to replace the distributed load with some modelling requirements.

The vacuum chamber method can provide a good simulation of uniform-distributed wind loading acting on roof sheeting, but tests are

expensive and time-consuming due to the manufacture of the vacuum chamber system. The air bag method has the apparent advantage of both distributed load simulation and economy, but there may be some doubt as to load uniformity over the roofing surface since light gauge metal roofing sheets usually have complex profiles and are flexible. It is believed that the midspan load method is less expensive and easy to perform in a common structural laboratory, and therefore this method has been used in consulting jobs (Reardon, 1980).

As indicated in Technical Record 440 (EBS, 1978), it is considered a basic requirement in the midspan load method that the magnitude of the maximum load per fastener and bending moment at the critical support must be modelled correctly, and that the test specimen should be so constructed that the loads are transmitted to the fasteners in a realistic fashion. The definitions of the maximum load per fastener and bending moment at central support in the above basic requirement were based on simple beam theory rather than on shell theory. To comply with the first part of the requirement, the currently used method is to adjust both roofing span length and line load magnitude based on a two-span continuous simply supported beam (or simple plate with one-way bending). Fig. 2.3 schematically shows this kind of adjustment process. As for the load transmission requirement, a properly designed loading pad is necessary.

In this investigation, the midspan load method was chosen due to practical limitations associated with the use of a commercial hydraulic testing machine. The basic requirement involving in the midspan load method was also discussed in terms of some relevant experimental results. The basic roofing spans in the test were 650 mm and 870 mm, which are equivalent to prototype end spans of approximately 900 mm and 1200 mm, respectively, according to the aforementioned equivalent method. The width of the tested roofing sheets was selected as large as possible within the physical limitation of the testing machine and with the consideration of reasonable comparison between three types of roofing sheets. A summary of different type tests, associated with roof sheeting profiles, roofing spans, fasteners and sheeting thicknesses, is given in Table 2.1. During assembling the tested roof systems, all screws were tightened until the neoprene washers were just prevented from rotating to avoid either over-tightened or loose screws. Attempts were made to ensure that all the screws were located exactly at the centre of the sheeting crest and perpendicular to the plane of sheeting. High quality timber was used in all the tests to prevent premature screw withdrawal from the timber battens.

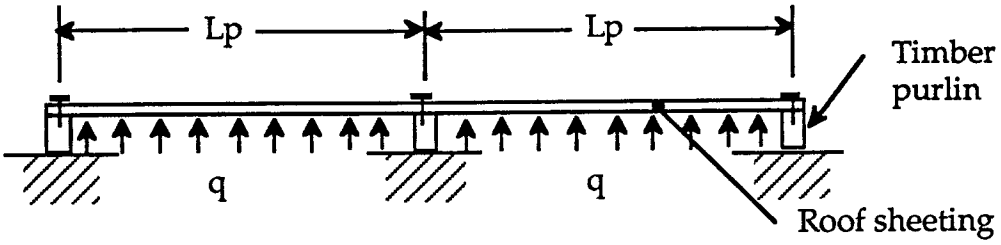

(a) Prototype

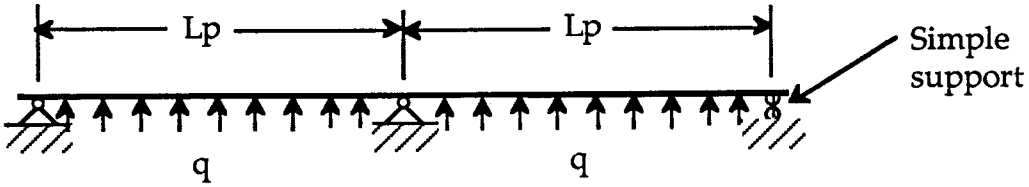

(b) Mechanical Model of Prototype

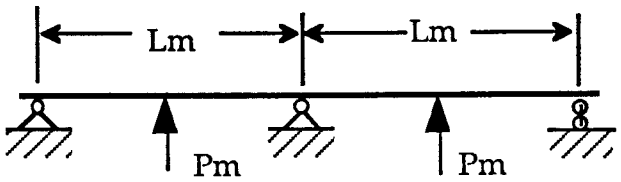

(c) Equivalent Model used in Midspan Load Method

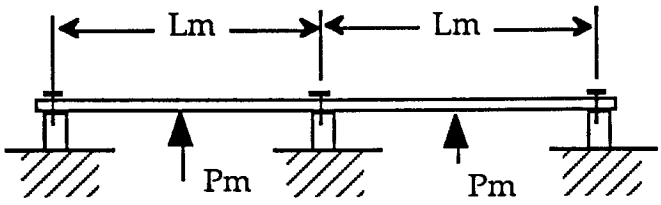

(d) Test Model

FIGURE 2.3 MODELLING PROCESS IN MIDSPAN LOAD METHOD

TABLE 2.1 ROOFING ASSEMBLY DETAILS IN THE TEST

Sheeting Profile	Width x Thickness (TCT) (mm)	Cyclone Washers	Number of Fasteners	Equivalent Spans (mm)
Custom Orb	580 x 0.47	No	4	900
Custom Orb	580 x 0.47	Yes	4	900
Custom Orb	580 x 0.47	No	4	1200
Custom Blue Orb	580 x 0.66	No	4	900
Spandek	500 x 0.47	No	3	900
Spandek	500 x 0.47	Yes	3	900
Spandek	500 x 0.47	No	3	1200
Spandek	500 x 0.53	No	3	900
Trimdek	550 x 0.47	No	3	900
Trimdek	550 x 0.47	Yes	3	900
Trimdek	550 x 0.47	No	3	1200

2.3 Test Rig

The test rig used in the present investigation was similar to that designed by Mahendran (1990), as shown in Fig. 2.4. A servo-controlled hydraulic testing machine (INSTRON) of 200 kN static capacity was a major component of the test rig. The timber battens at both ends of the roof sheeting were fixed to the machine frame via two large steel beams. The central timber batten was supported by a small steel frame which was clamped in the stationary jaw fixed to the Instron machine load cell. Two loading pads were fixed a steel beam which was connected to the movable ram of the Instron machine. Between the beam and the movable ram there was another load cell (KYOWA) of 20 kN capacity.

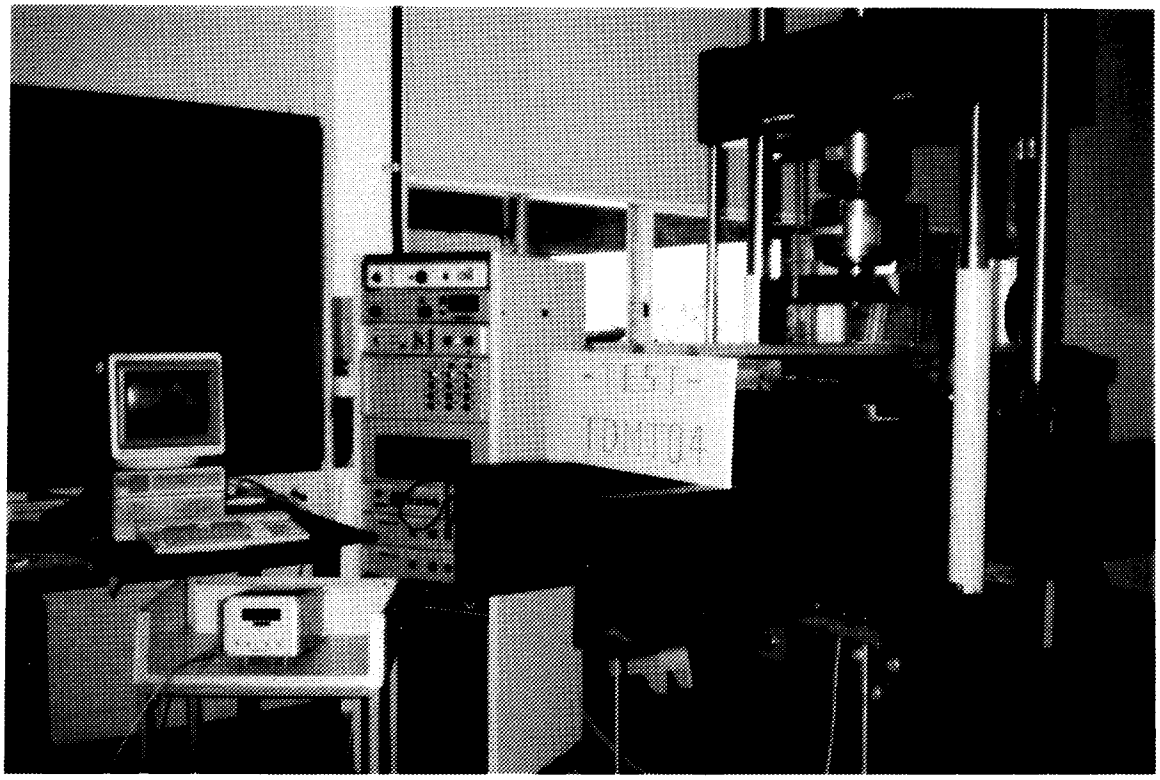

FIG.2.4 TEST RIG

Flexible rubber loading pads were used to apply line loads to the underside of the roofing sheets. The upper face of the loading pads was formed to coincide in general with the shape of the roof sheeting profiles. For the arc-tangent type roofing sheet, a thin rubber tube filled with water was fixed to the top of the rubber loading pads to ensure uniform pressure was applied during the whole testing process. Similar loading method was used by Beck and Stevens (1979). However, it should be noted that such loading pads might develop additional restraints to the cross-sectional deformation of roofing sheets and create friction forces between rubber pads and sheeting surface. Correspondingly, the measured results of ultimate load of roofing claddings may be overestimated. A discussion of this loading method is conducted in Section 6, based on some testing results.

2.4 Measurement and Test Procedure

The Instron load cell was used to measure the fastener reaction at the central support. The average load per fastener was obtained by dividing the

total reaction force by the number of fasteners at the central support. The Kyowa load cell was employed to measure the total wind uplift acting on the roofing sheet. The equivalent average pressure over the surface of the sheeting was estimated in terms of the mechanical model of the roofing assembly shown in Fig. 2.3 and the measured total wind uplift. The Instron load cell was calibrated against the Kyowa load cell by using a set of springs with proper stiffness. The calibration was found to be satisfactory and the results were plotted in Fig. 2.5. In such arrangement, the relationship between the fastener reaction force at the central support and the wind uplift can be directly determined so that the assumption of the simply supported conditions in the roofing assembly model can be examined.

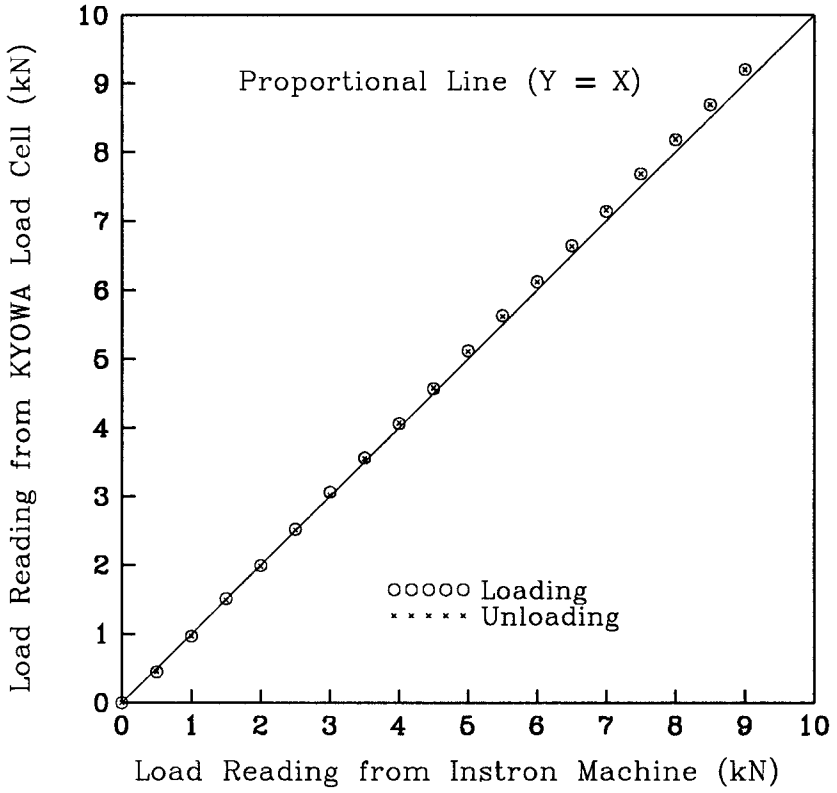

FIG.2.5 LOAD CELL CALIBRATION OF INSTRON MACHINE

Four dial gauges graduated to 0.01 mm were arranged at screwed crests and unscrewed crests or pans of roofing sheets to measure upward deflections. When a repeated load was applied to the roofing to obtain loading-unloading properties at the different deflection stages or cyclic load-deflection properties, a displacement transducer and X-Y recorder were used. The test rig and instrument arrangement are schematically shown in Fig. 2.6.

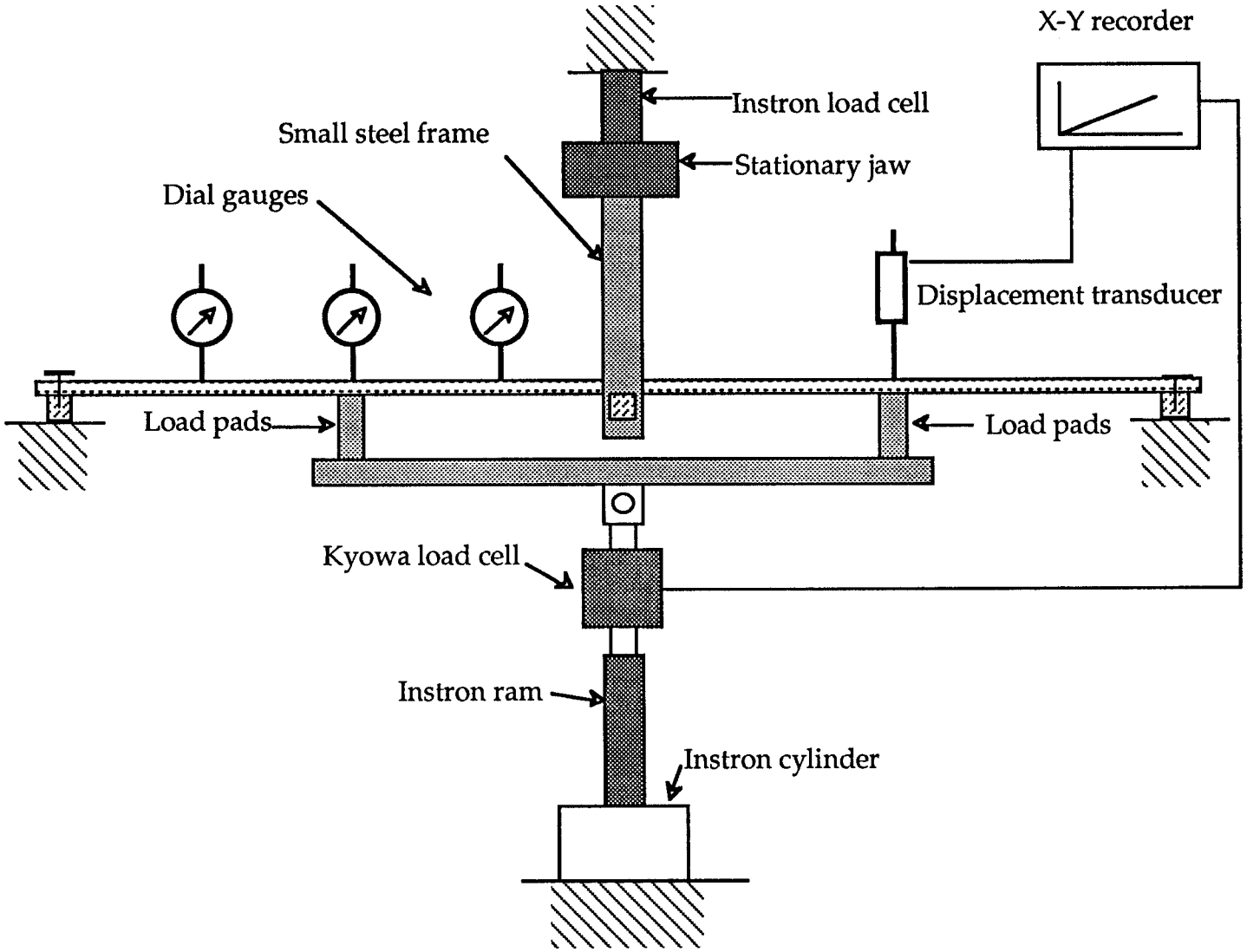

FIGURE 2.6 SCHEMATIC VIEW OF TEST ARRANGEMENT

All tests were conducted by controlling the displacement of the movable ram of the Instron machine in order to follow the entire loading path through any unstable localised failure stages. The calibration results of the ram displacement versus digital number from Instron's position display unit are given in Fig. 2.7. In the roof sheeting tests, the deflection measurement was taken at each increment of 200 N until the vicinity of localised failure when the load was measured at specific intervals of deflection. When the cyclic load tests were conducted, a microcomputer HP9122 controlled the cyclic tests via an intelligent interface with a computer program " CYCLES5". A brief description of the cyclic tests is given in Section 4.3.

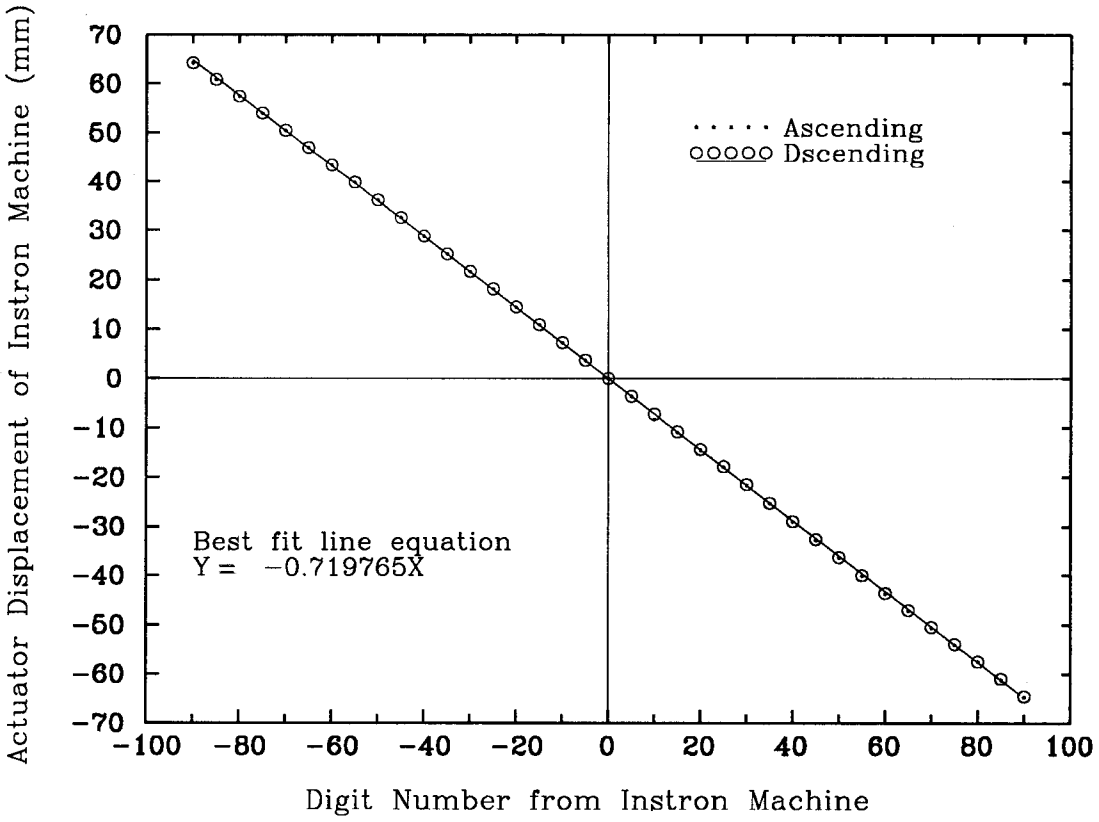

FIG.2.7 DISPLACEMENT CALIBRATION OF INSTRON MACHINE

3. SHEETING MATERIAL PROPERTIES

The structural behaviour of light gauge steel roofing greatly depends on material properties of roofing sheets. The roofing material properties are also a basis for further finite element analysis of roofing assemblies. Therefore, tensile tests of roof sheeting material were conducted to determine some important properties specified by Australian Standard (SAA, 1991).

3.1 Test Pieces and Methods

Tensile test pieces were taken from the sample flat plates which were supplied by the roofing manufacturers and taken at intervals during the rolling of the regular roofing sheets used in this investigation. Because the roofing sheets were cold-formed, the test pieces from the flat plates were cut in groups and their longitudinal axes were either at right angles or parallel to the direction of final rolling of the roofing sheets. The basic dimensions of the test pieces are shown in Fig. 3.1.

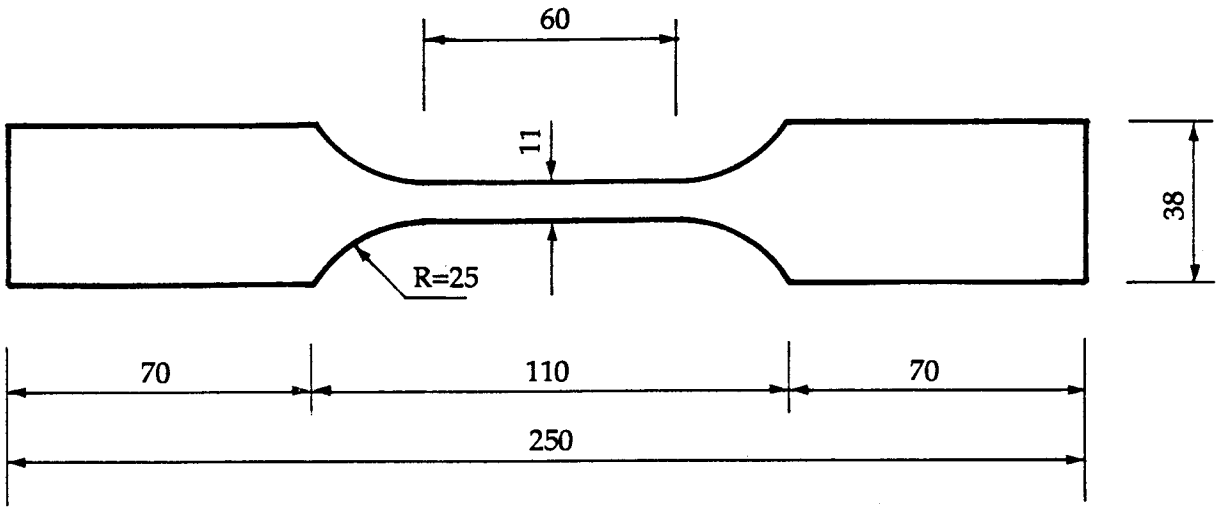

FIG. 3.1 DIMENSIONS OF TENSILE TEST PIECES (mm)

The tensile tests were conducted on the Instron 4300 Series Universal Testing Machine of 10 kN capacity. A X-Y recorder which was connected to the control console of the machine was used to plot the force-extension curves, or force-strain curves when an extensometer was used. Fig. 3.2 shows this test set-up. In testing, the extensometer gauge length was set for 50 mm, and several strain rates were used to determine whether or not the strain rate affected the material properties. Before testing, the width of test pieces at the central section was individually measured by using a micrometer. The thicknesses of several pieces were measured by an electron microscope fitted with a x-ray diffraction composition analysis system to identify both base metal and coating thicknesses. A total of 30 pieces were tested for both longitudinal and transverse directions.

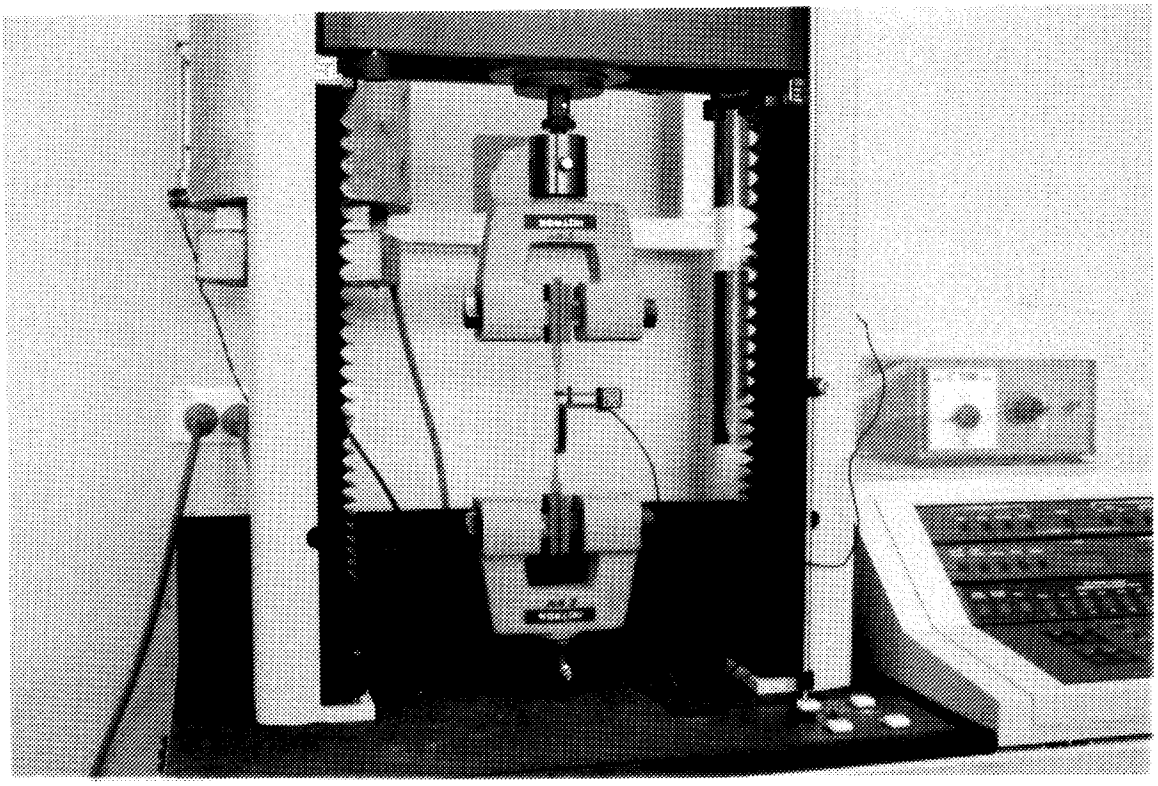

FIG.3.2 TENSILE TEST ARRANGEMENT

3.2 Properties in Longitudinal Direction

A typical stress-strain curve obtained by using the extensometer is shown in Fig. 3.3. The calculation of the stress in Fig. 3.3 was based on the base metal thickness of 0.42 mm specified by the manufacture. The mean measured base metal thickness was 0.43 mm. At the beginning of the tensile test, the relation between stress and strain is linear, and the Young's modulus was about 214,300 MPa. Then the curve became nonlinear until the stress reached a value of 739MPa. After that point (point A), the stress remained approximately constant while the strain increased rapidly. This yield phenomenon was followed by a rapid stress reduction and an abrupt break. Due to lack of strain hardening, the ultimate strength of the sheeting material was the same as the yield stress. If a permanent strain of 0.002 was adopted to define a nominal yield stress, the nominal yield stress was 710MPa, which was still close to the ultimate stress. The elongation after fracture (total elongation) was 1.93%, and based on the total elongation, the estimated strain rate was about 9.5×10^{-5}. From the repeated tests, it was found that the

variation of the measured yield stress was small, but the total elongation was possibly larger than 2%. It also found that a larger strain rate of 9.5 x 10^{-4} did not significantly affect the material properties. Fig. 3.4 shows some force-extension curves using a strain rate of 9.5 x 10^{-4}.

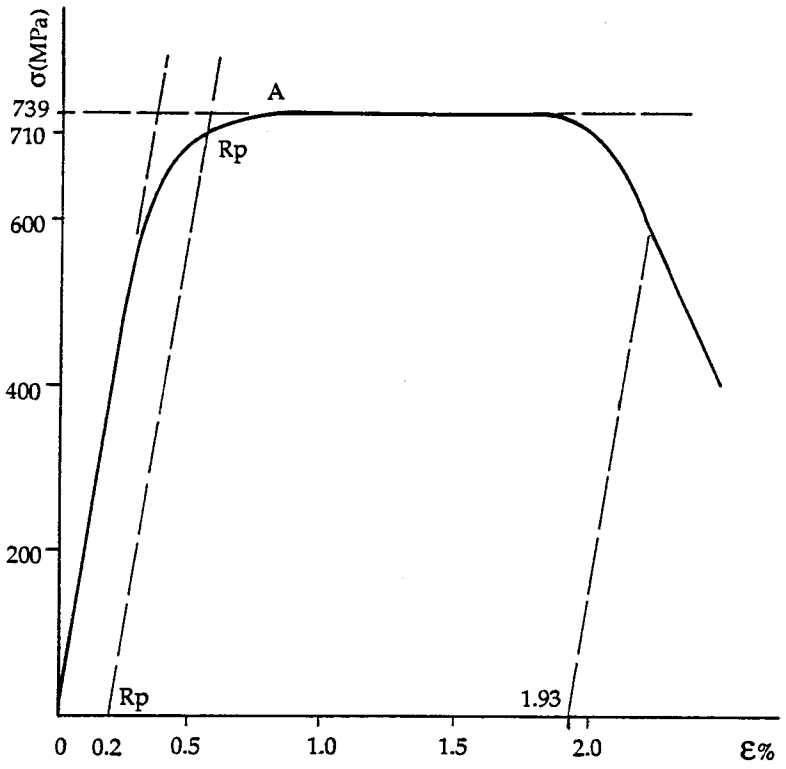

FIG. 3.3 STRESS-STRAIN CURVE IN LONGITUDINAL DIRECTION

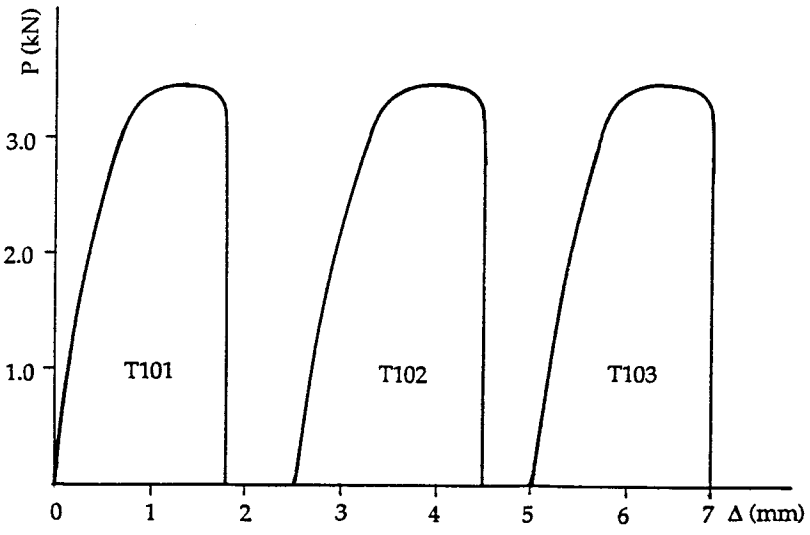

FIG. 3.4 LOAD-EXTENSION CURVE IN LONGITUDINAL DIRECTION

3.3 Properties in Transverse Direction.

Some properties of the sheeting material in the transverse direction were found to be different from those in the longitudinal direction. The ultimate strength or the nominal yield stress was higher than that in the longitudinal direction, and the total elongation was much lower. The Young's modulus was measured as 234,000 MPa. Fig. 3.5 shows a typical stress-strain curve in the transverse direction. In this sample, the ultimate strength was 822 MPa while the total elongation was only 0.5%. As a result, the material showed a brittle nature of failure. From the force-extension tests, the material properties in transverse direction were found to be stable, as shown in Fig. 3.6.

In summary, the sheeting material had a high tensile strength in both directions. The Young's elastic modulus was similar to those of most steel materials. In the longitudinal direction, the sheeting material appeared to be a plastic material and the stress-strain curve could be represented by an elasto-plastic curve without strain hardening. In the transverse direction, the sheeting material approached a brittle material and the elasto-plastic model without strain hardening only was an approximation.

4. BEHAVIOUR OF DIFFERENT PROFILED ROOFING SHEETS

4.1 Deflection Behaviour and Failure Modes

4.1.1 Arc-tangent type roofing sheet (CUSTOM ORB profile)

The upward deflections of the arc-tangent type roofing sheet at four points were plotted in Fig. 4.1 against equivalent average wind pressure. The curves were obtained by monotonic tests. The deflections were normal to the plane of the roofing sheet and the corresponding positions of the measured points are showed in Fig. 4.2. The calculation of equivalent average wind pressure was based on the modelling requirement as mentioned in Section 2.2. Besides such monotonic tests, a multi loading-unloading test was conducted to enhance the understanding of structural behaviour of the roofing sheets by using displacement transducer and x-y recorder. Fig. 4.3 shows loading-unloading curves at point A. In Fig. 4.4, cross-sectional distortion evolution of one corrugation passing through the points A and D under different loads was approximately exhibited, based on the measured deflection values of points A and D as well as observation during the testing.

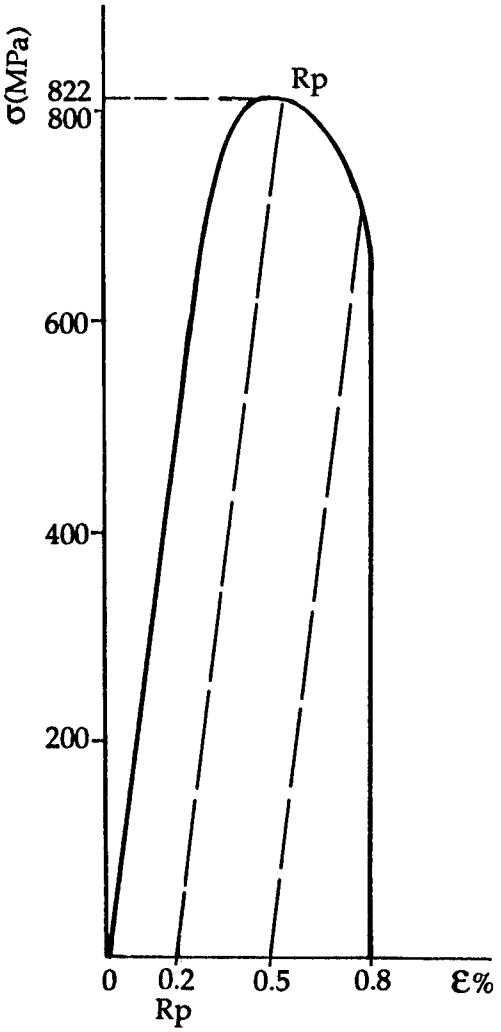

FIG. 3.5
STRESS-STRAIN CURVE IN TRANSVERSE DIRECTION

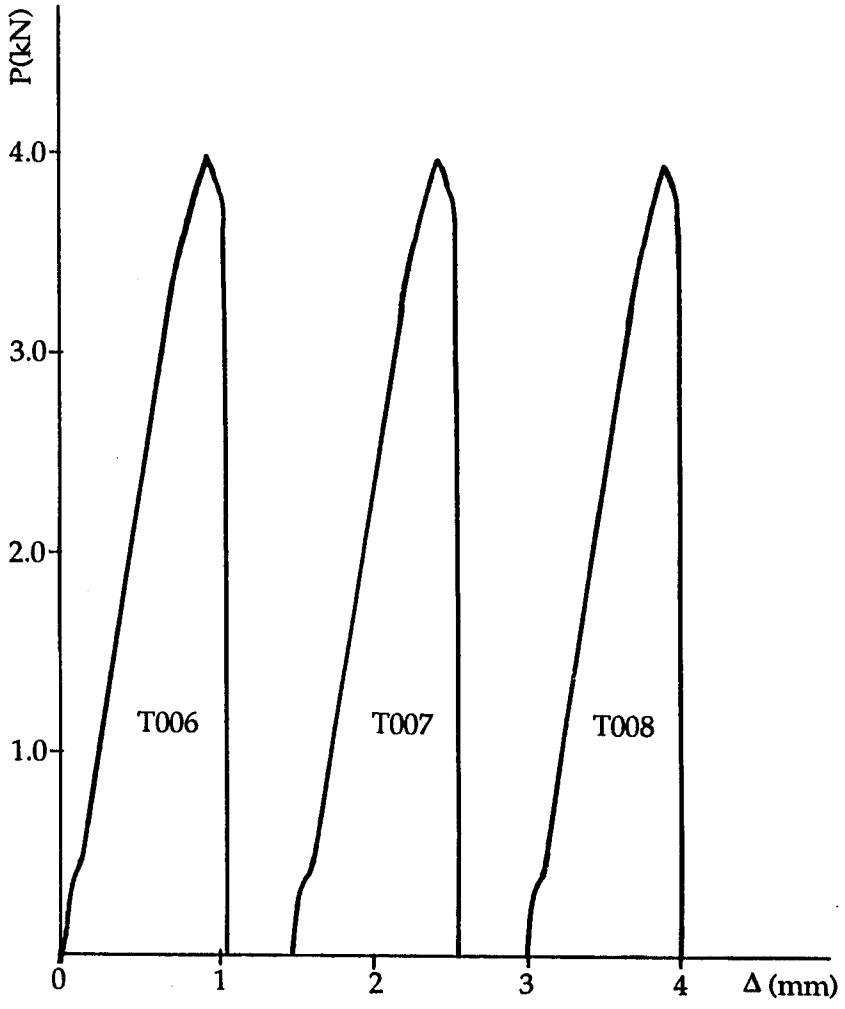

FIG. 3.6 LOAD-EXTENSION CURVE IN TRANSVERSE DIRECTION

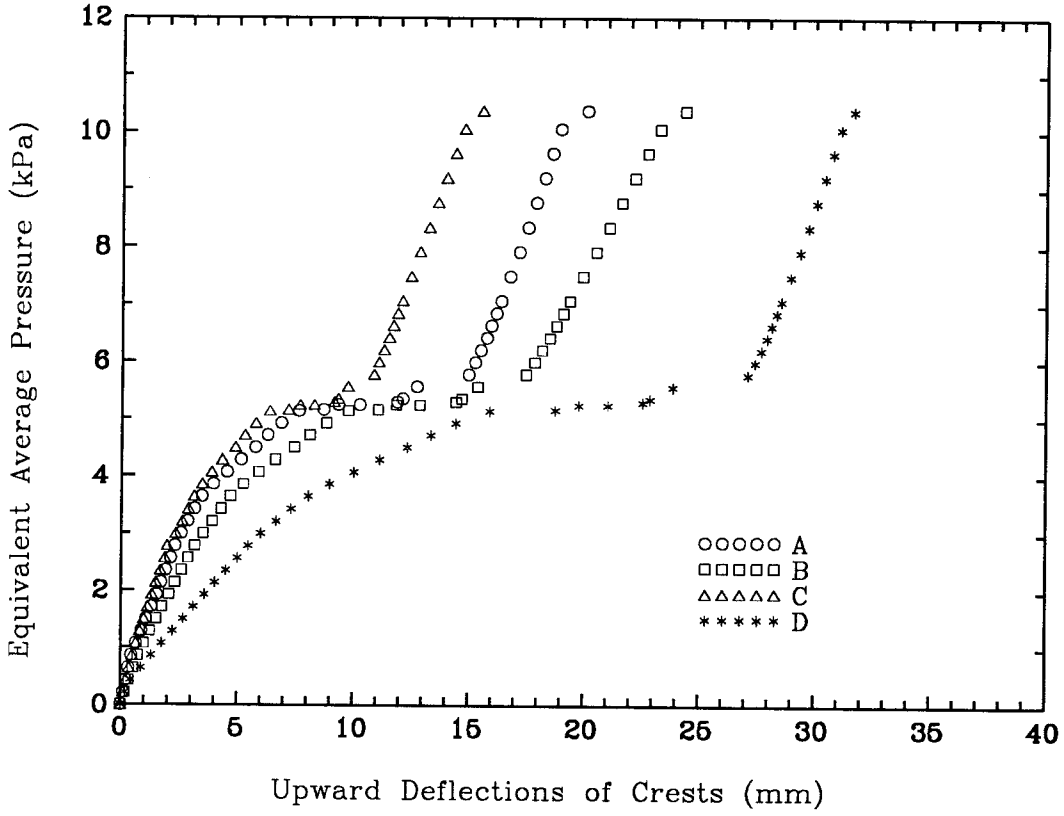

FIG.4.1 LOAD-DEFLECTION CURVES OF ARC-TANGENT TYPE ROOFING SHEET

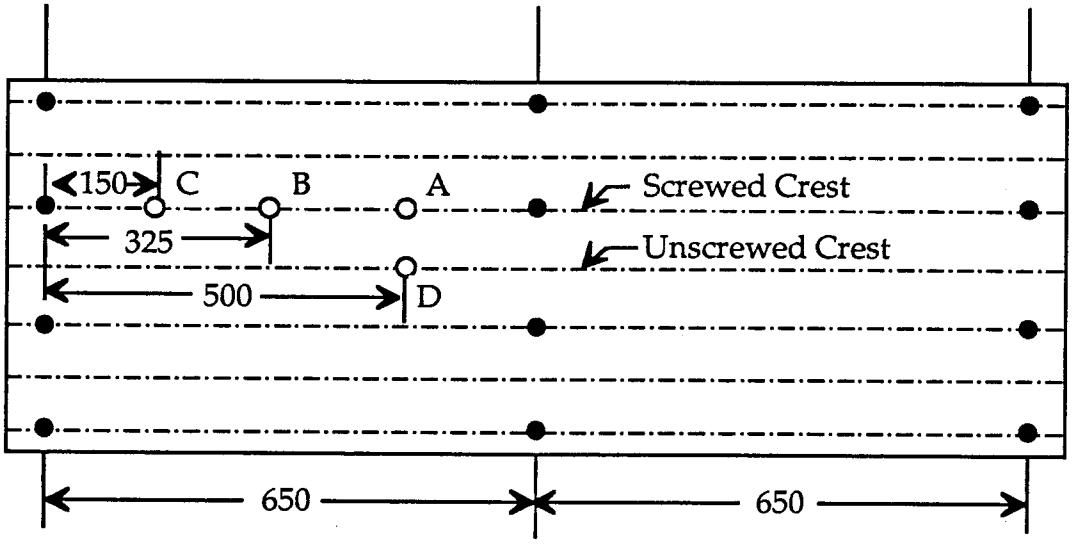

FIGURE 4.2 GENERAL POSITIONS OF MEASURED DEFLECTION POINTS

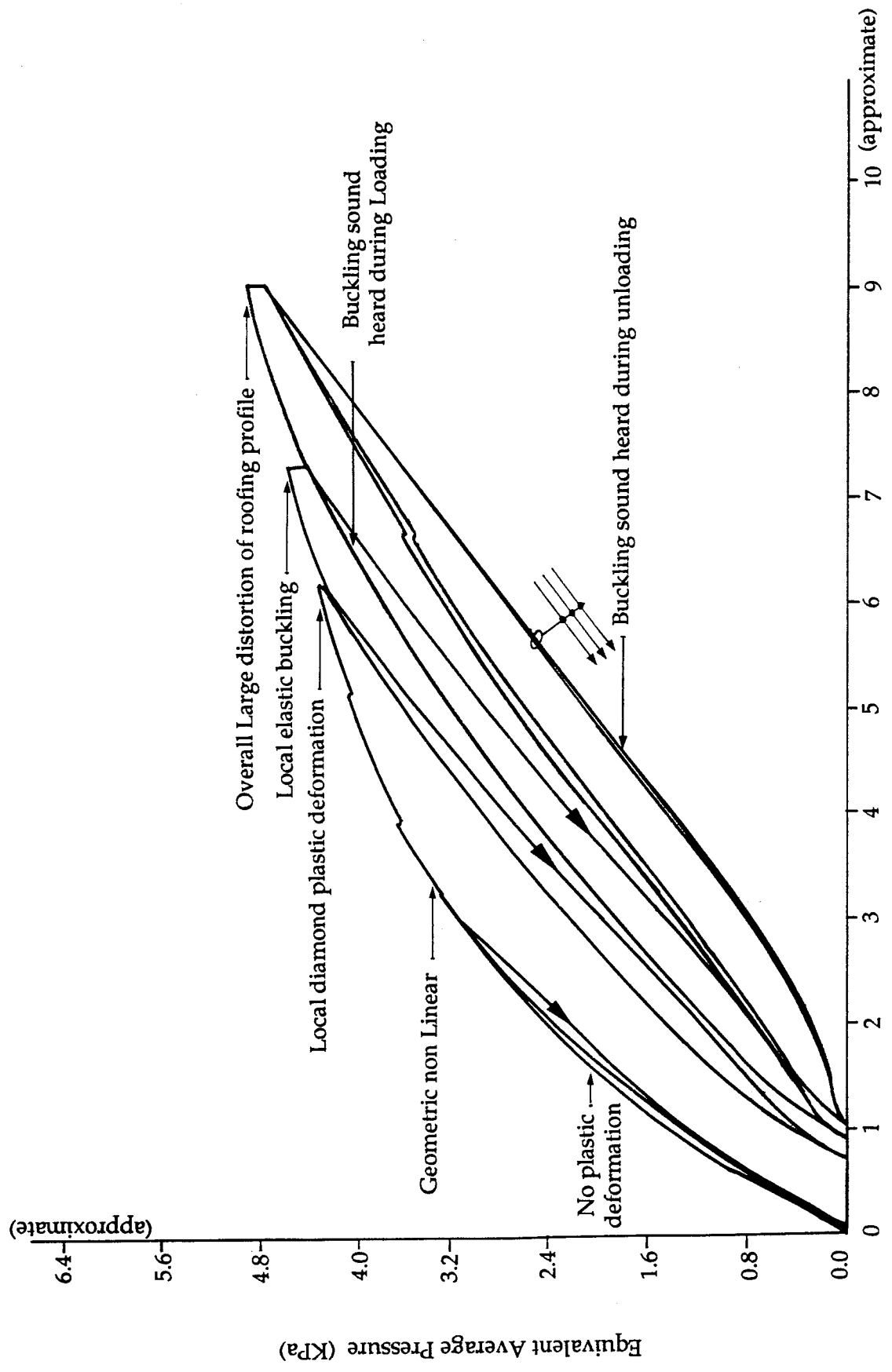

FIG. 4.3 LOADING AND UNLOADING OF ARC-TANGENT TYPE ROOFING SHEET

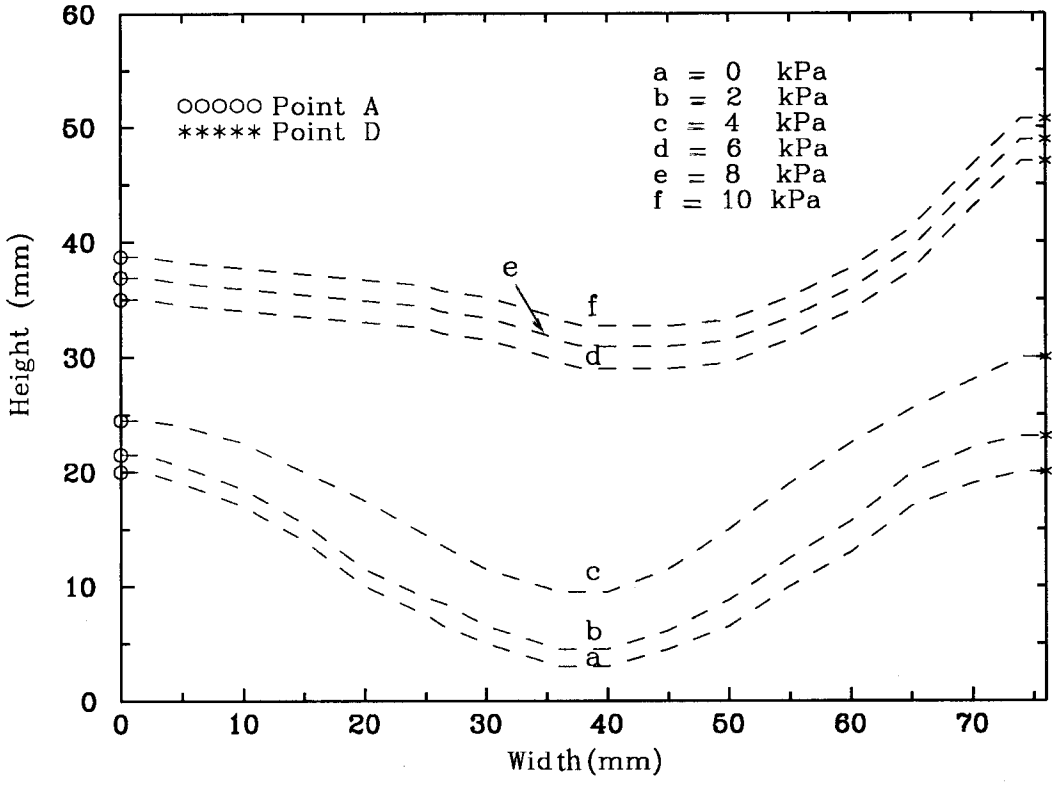

FIG.4.4 CROSS-SECTIONAL DISTORTION OF ONE CORRUGATION OF ARC-TANGENT TYPE ROOFING SHEET

When the equivalent wind pressure was below 1.2 kPa, the structural behaviour of the arc-tangent type roofing sheet was approximately linear and elastic. With the increase of loading, there was a change in the sheeting geometry. The upward deflection of the unscrewed crest was larger than that of the screwed crest (see Fig. 4.4). This geometric distortion caused a geometric nonlinear characteristic in the structural behaviour of the light gauge steel roofing sheet so that the slope of load-deflection curves, as shown in Figs. 4.1 and 4.3, was not constant. However, if the equivalent wind pressure was below 3.2 kPa, the arc-tangent type roof sheeting behaviour still remained approximately elastic since there was only a small permanent plastic deformation after unloading (see Fig. 4.3).

With the further increase of loading, a local diamond-shaped deformation (see Fig. 4.5) progressively developed at each screwed crest at the central support under the head of the screw fasteners. This local deformation was plastic and affected overall sheeting deformation so that there was a permanent plastic deformation appearing in Fig. 4.3 after unloading, and a hysteresis loop formed during the loading-unloading process. When the load increased to an equivalent pressure greater than 4.5

kPa, a local buckle with a clear sound occurred around the screw fasteners at the central support, which caused a sudden small drop of loading. The hysteresis loop area at this stage became larger, which reflected an increase of lost energy. The local plastic buckling was followed by an overall cross-sectional distortion at the central support without any load increase. Correspondingly, the load-deflection curve exhibited an abrupt flattening, which means the roofing sheet was yielding. This initial failure occurred at an equivalent pressure of around 5 kPa. It was interesting to find that this large cross-section distortion was mainly elastic because large permanent plastic deformation was not found after unloading. Also no cracks were obvious during the large distortion of the roofing sheet.

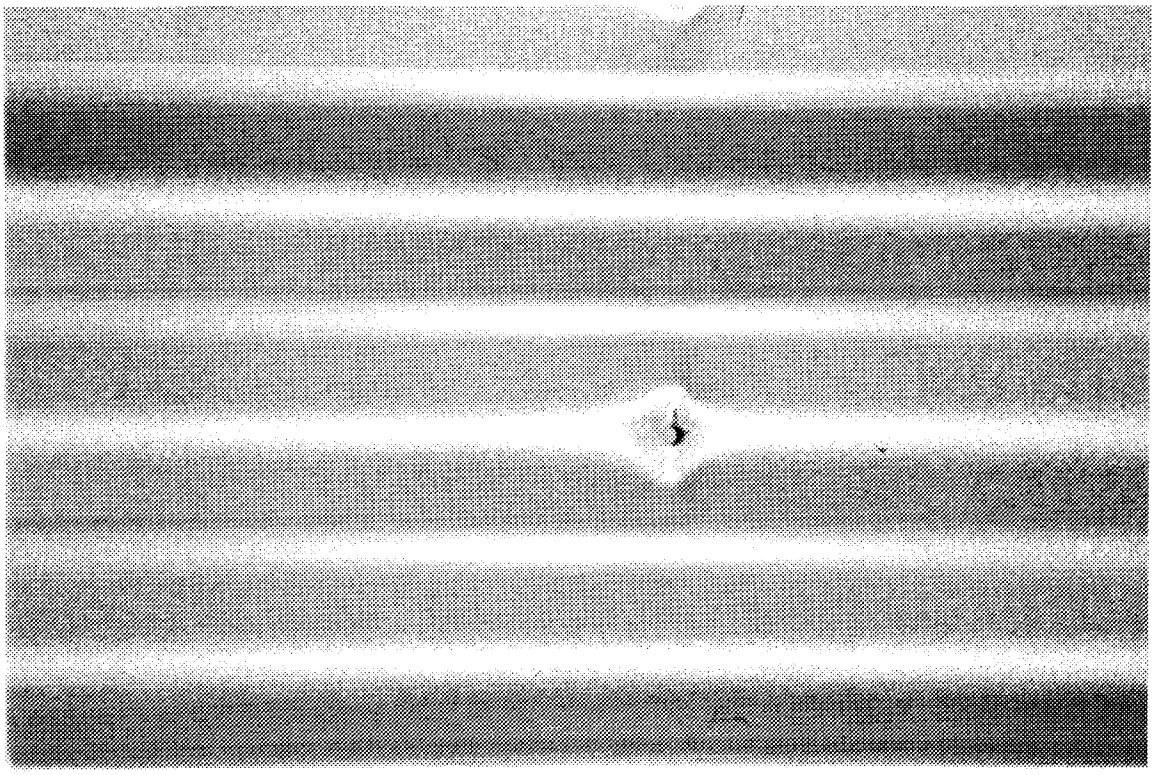

FIG. 4.5 LOCAL PLASTIC DEFORMATION OF ARC-TANGENT TYPE ROOFING SHEET

After the screwed crests around the fasteners at the central support were totally flattened, a different roof sheeting profile and a new stress distribution probably formed, which caused a change in the structural behaviour. That is, the structural stiffness of the roofing sheet suddenly increased from a value of nearly zero, and an approximate linear relation

between the load and deflection appeared. Obviously, this deflection hardening behaviour was not related to strain hardening in material behaviour as some other structures because the sheeting material used herein had no strain hardening property. Until the loading increased to more than an equivalent pressure of 9.5 kPa, the overall cross-sectional buckling along the midspan loading pads occurred. This final failure mode, however, was due to midspan load method and probably was not expected in the prototype roofing sheet. It is obvious that the simple elastic beam theory is unable to predict such complicated structural behaviour and even deflection difference among the measured four points shown in Fig. 4.1.

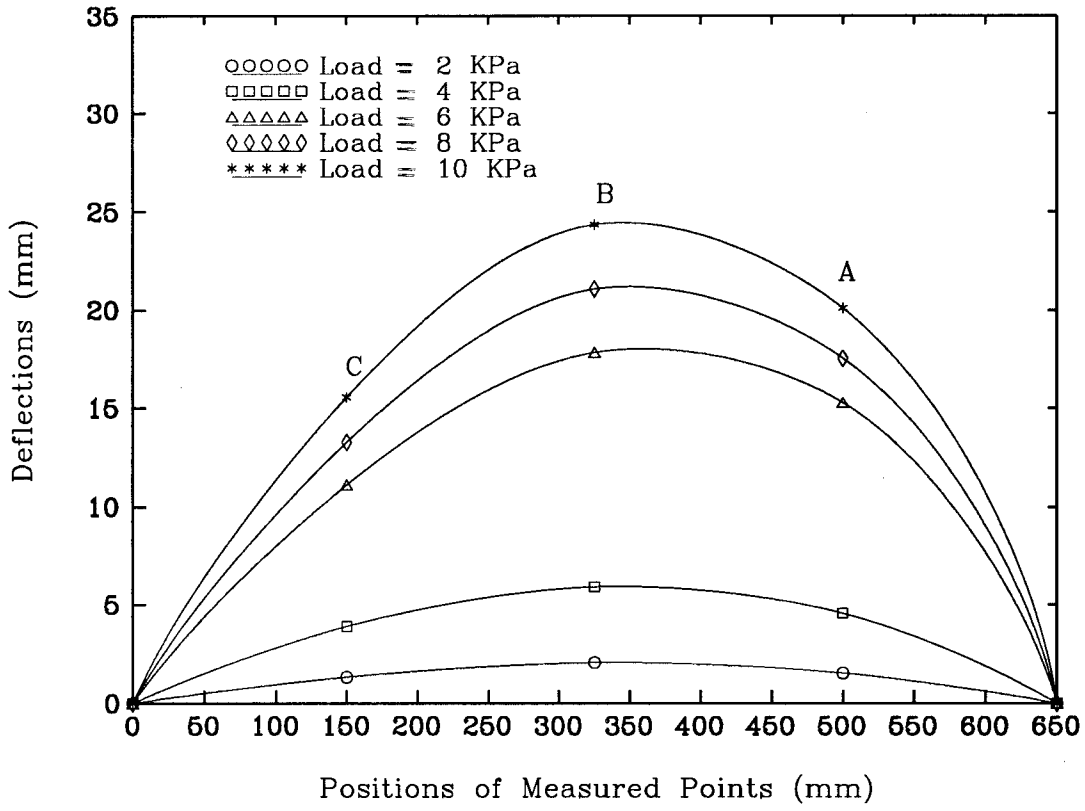

FIG.4.6 DEFLECTION OF THE SCREWED CREST IN LONGITUDINAL DIRECTION OF ARC-TANGENT TYPE ROOFING SHEET

While Fig. 4.4 shows a cross-sectional distortion of one corrugation, Fig. 4.6 shows the deflection of the screwed crest of the roofing sheet in longitudinal direction. Only one span deflection was plotted and the coordinate of 650 mm represented the central support location. As the curves were plotted at a regular interval of 2 kPa equivalent pressure, the space change between two curves with loading increase can indicate the change of

roofing behaviour. The space between the first curve and the second curve was larger than that between the first curve and X-axis. This means that the roofing deflection was not linear from the first load grade to the second load grade. The rapid increase of the space between the second and third curves reflected a strong nonlinear characteristic while the rapid decrease of next space indicates an increase or restoration of roofing stiffness. It is also obvious that the deflection at point A (next to the central support (see Fig. 4.2) was larger than that at point C (next to the end support) after the large cross-sectional distortion of the roofing sheet.

4.1.2 Trapezoidal type roofing sheet (SPANDEK profile)

The upward deflections of the trapezoidal type roofing sheet at four points are shown in Fig. 4.7. The relevant loading-unloading curve is shown in Fig. 4.8. The positions of the deflection of the measured points were similar to the arc-tangent type roofing case.

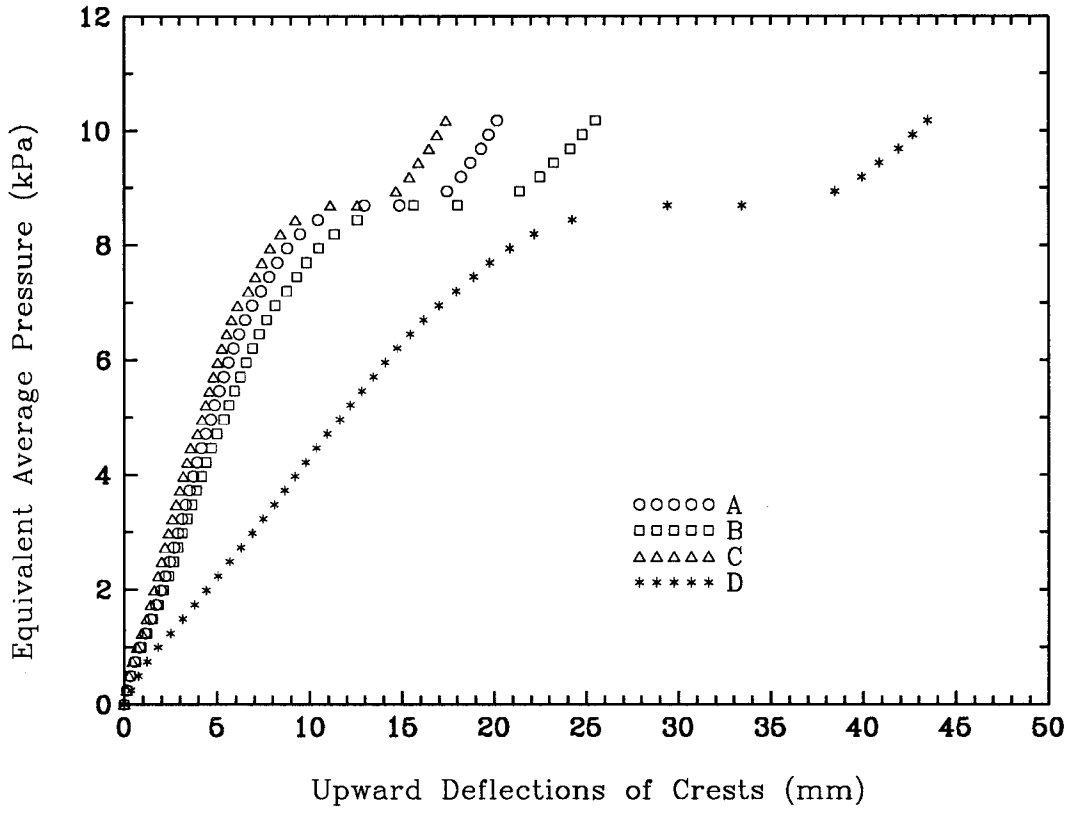

FIG.4.7 LOAD –DEFLECTION CURVES OF TRAPEZOIDAL TYPE ROOFING SHEET

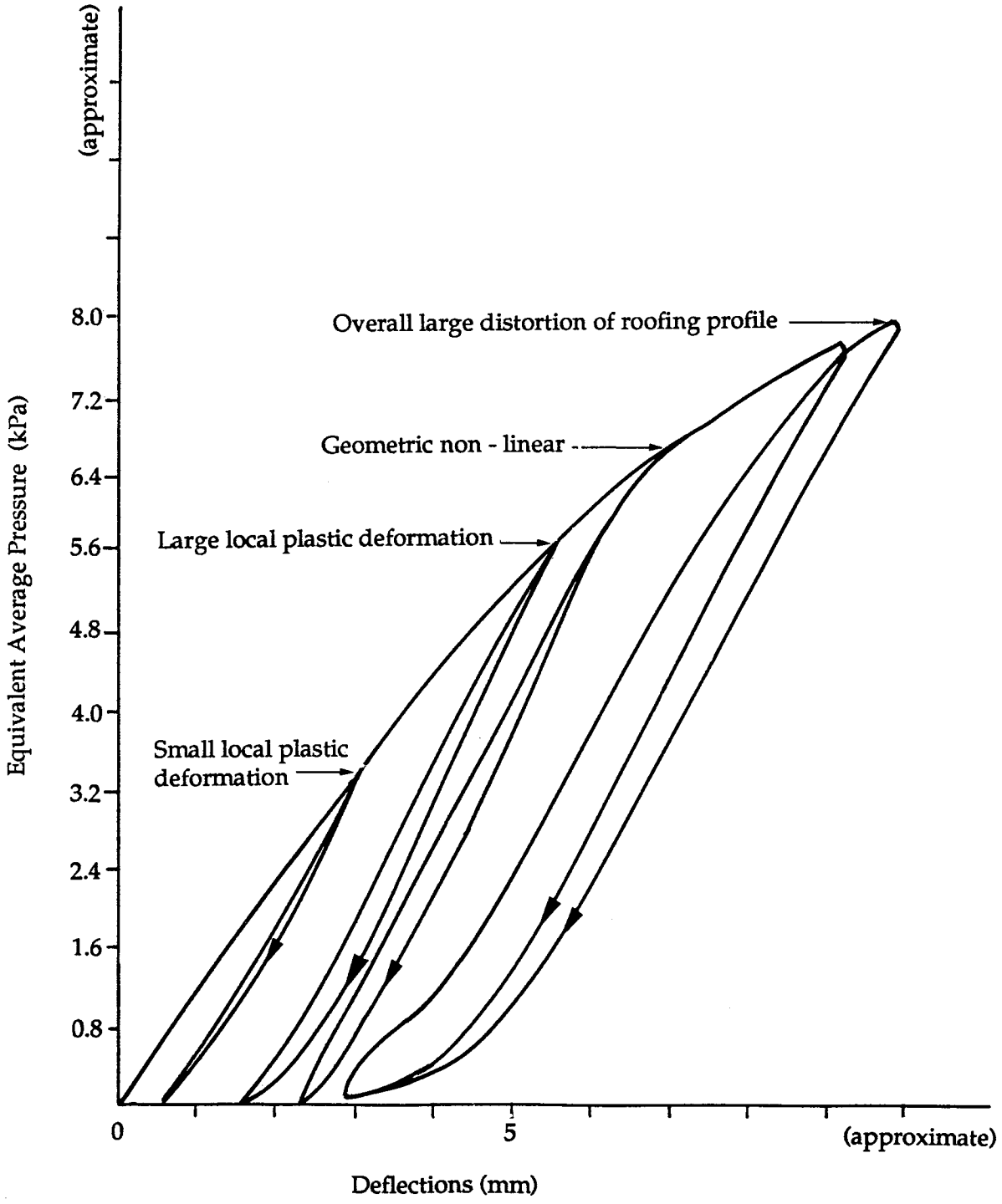

FIG. 4.8 LOADING AND UNLOADING OF TRAPEZOIDAL TYPE ROOFING SHEET

Although the load-deflection curves shown in both figures seem to be linear until an equivalent pressure of about 5 kPa, small plastic dimples at the screwed crests at the central support under the head of the screw fasteners began at a lower pressure of around 3 kPa. This local deformation led to a small hysteresis loop in Fig. 4.8. With the increase of uplift load, plastic dimple deformation on the top surface of the screwed crest at the central support developed progressively, with larger deformation in the longitudinal direction of the roofing. On two side surfaces of the screwed crest, the combined larger compression-bending stresses caused local plastic buckling to match the dimple formation (see Fig. 4.9). The local collapse was followed by a large cross-sectional distortion of the roofing sheet. When the equivalent pressure exceeded 8.5 kPa, the screwed crests at the central support became totally flat, as shown in Fig. 4.10. Correspondingly, the load-deflection curves exhibited an abrupt flattening, similar to the arc-tangent type roofing. This large distortion, however, was also basically elastic since the roofing sheet was not permanently deformed so severely after the unloading.

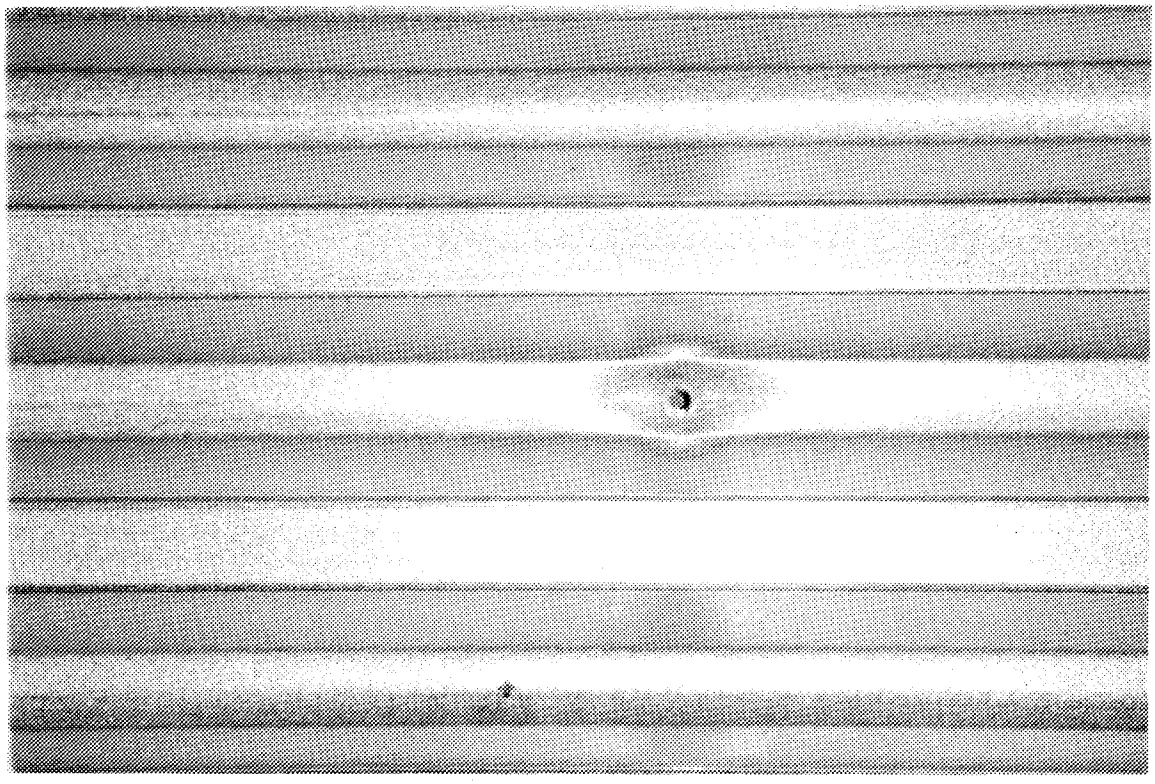

FIG. 4.9 LOCAL PLASTIC DEFORMATION OF TRAPEZOIDAL TYPE ROOFING SHEET

As the load continuously increased, the relationship between load and

deflection was approximately linear again. When the load reached an equivalent pressure of 9.2 kPa, buckling of wrinkle type appeared in sheeting valleys around the midspan load pads. Shortly, crippling collapse occurred cross the entire roofing width at the midspan of the sheet, which was similar to that described by Bushnell (1985).

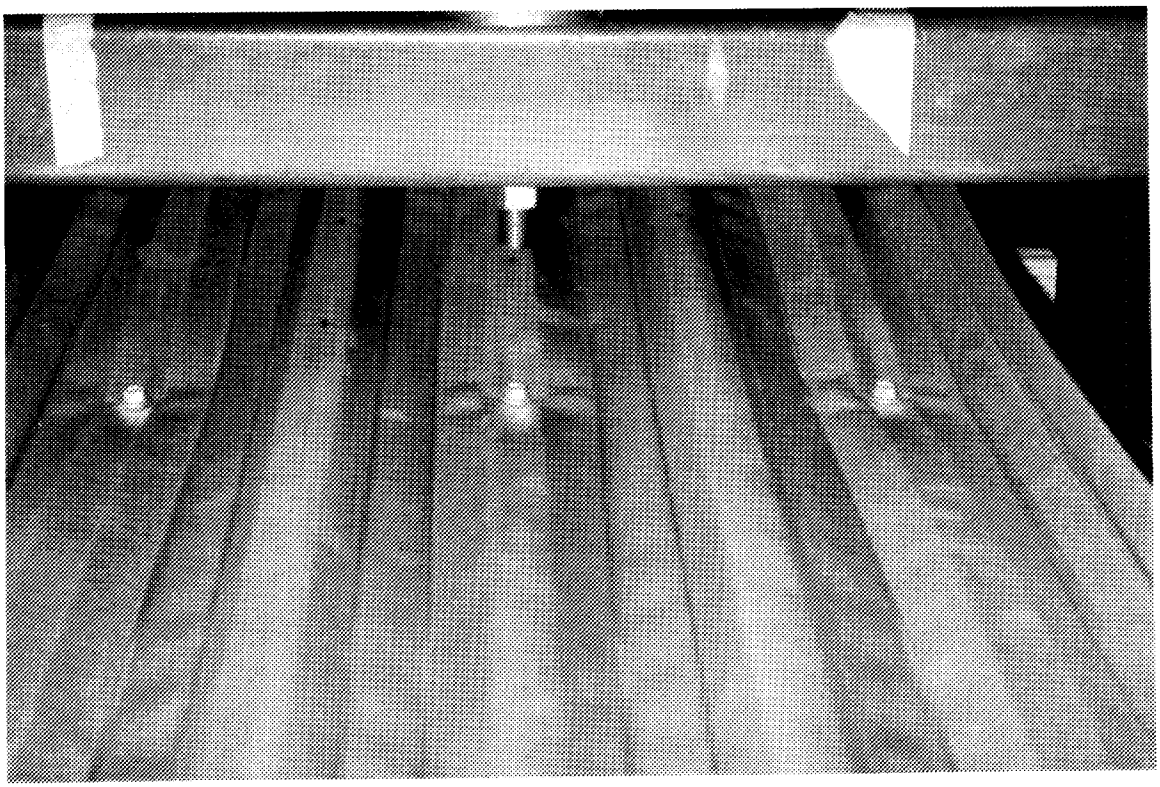

FIG. 4.10 LARGE CROSS-SECTIONAL DISTORTION OF TRAPEZOIDAL ROOFING SHEET

4.1.3 Ribbed type roofing sheet (TRIMDEK profile)

Ribbed type roofing sheets have a wide pan between two crests to allow more efficient drainage, compared with the other profiles. As for measured points, the middle line of the pan is equivalent to an unscrewed crest of the arc-tangent or trapezoidal type roofing sheet. Because of the wide pan, failure mode of the ribbed type roofing sheet was different from the other two types.

Fig. 4.11 shows the load-deflection curves at the four points, the positions of which were similar to those in Fig. 4.2. Fig. 4.12 shows the loading-unloading curve at point A. Under an equivalent pressure of less than 2 kPa, the deformation of roofing sheet was elastic. When equivalent

pressure increased to 3.6 kPa, a small plastic dimple appeared under the head of the screw fasteners at the central support, but caused a little influence on overall sheeting deformation as shown in Figs. 4.11 and 4.12. The area of the corresponding hysteresis loop was also very small, which indicated that there was no strong interaction between local and overall behaviour of the ribbed type roofing sheet. With the further increase of loading, the geometric deformation of roofing became obvious and the plastic dimples under the head of the screw fasteners became larger and larger, as shown in Fig. 4.13. The local plastic deformation of two sides of the crest, however, was not as large as those in the trapezoidal type roofing sheet. The overall permanent deformation and lost energy represented by hysteresis loop area were small as well. When the equivalent pressure reached about 7.6 kPa, the bottom surface of the plastic dimple under the internal fastener head suddenly split with a crack in the transverse direction of the roofing sheet. This indicated that there was a very large tension strain in the vicinity of fastener holes along the longitudinal direction of the crest. Compared with the other two type roofing sheets, there was no further large cross-sectional distortion, no yielding stage or deflection hardening stage. This is possibly attributed to the wide pan which could not provide a help to release the high tension stress at the screwed crest and to form a new stress distribution as the unscrewed crests of the other type roofing sheets could.

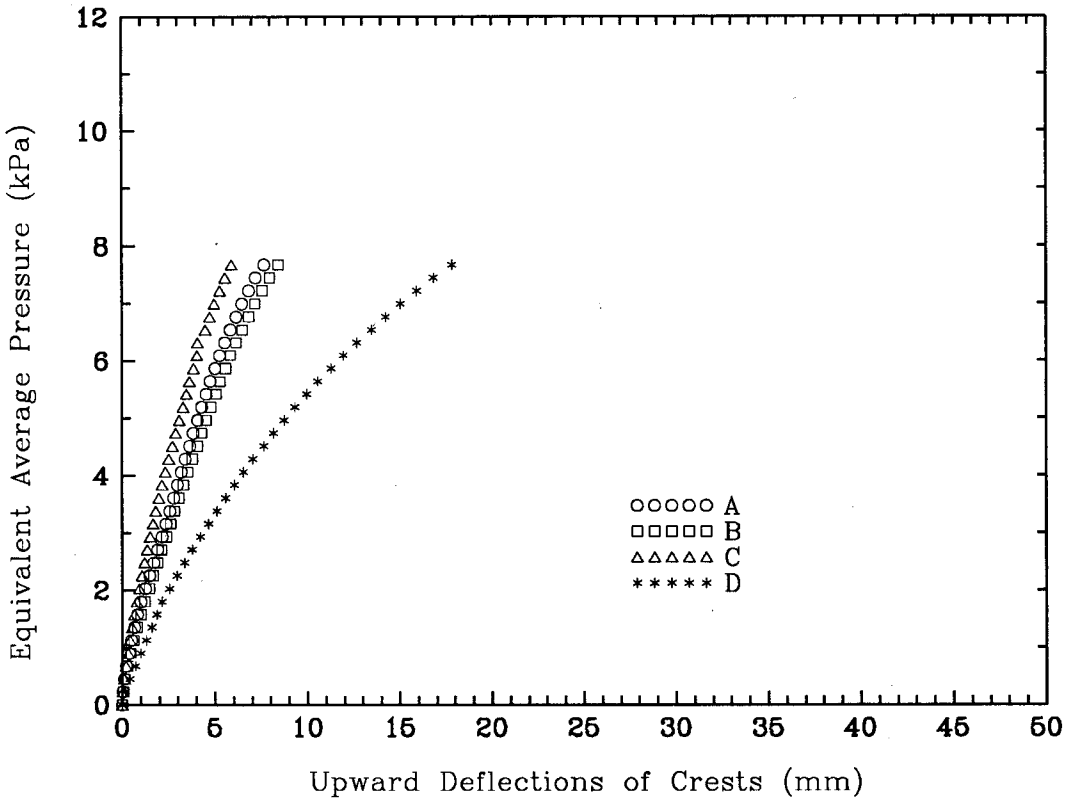

FIG.4.11 LOAD-DEFLECTION CURVES OF RIBBED TYPE ROOFING SHEET

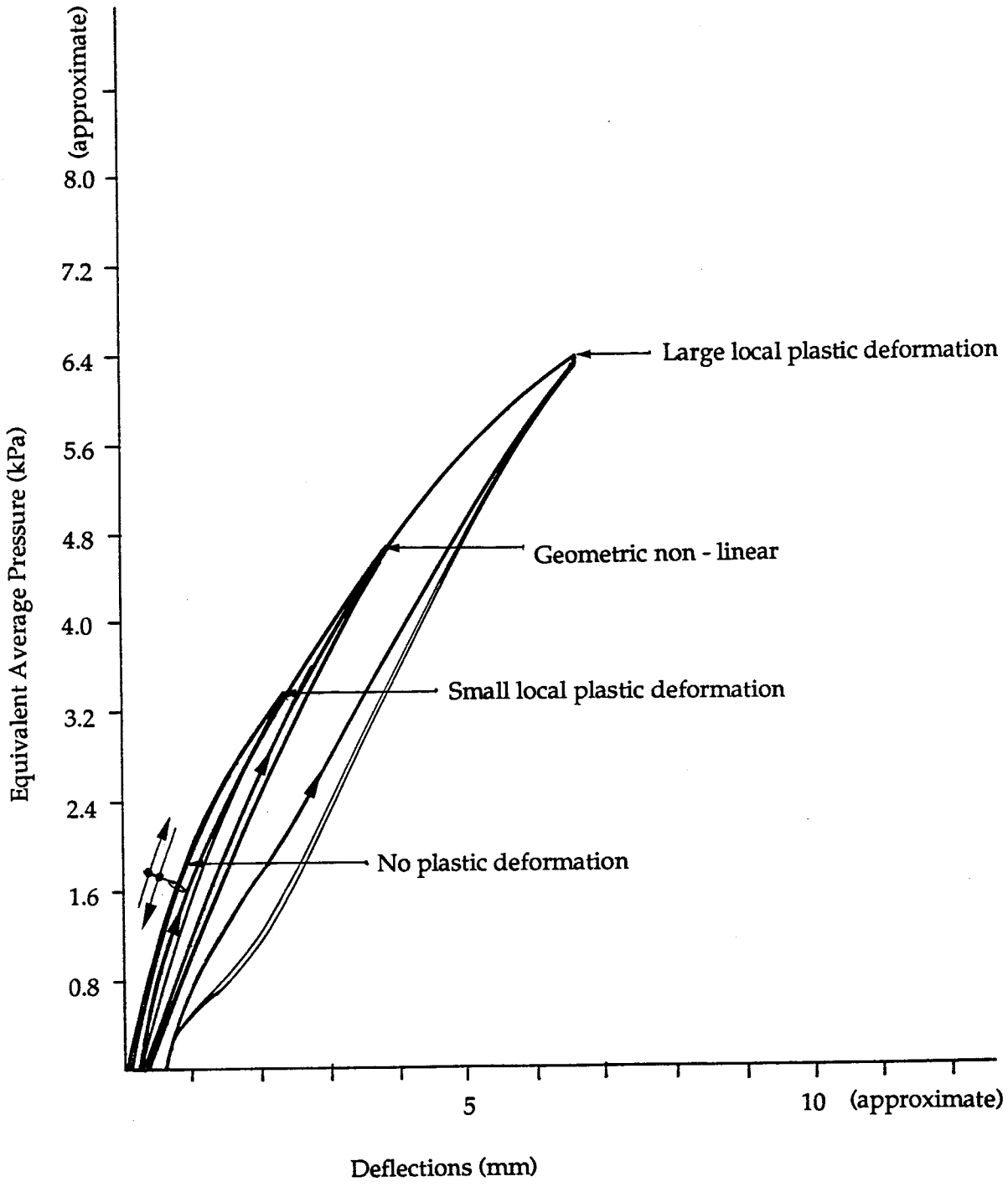

FIG. 4.12 LOADING AND UNLOADING OF RIBBED TYPE ROOFING SHEET

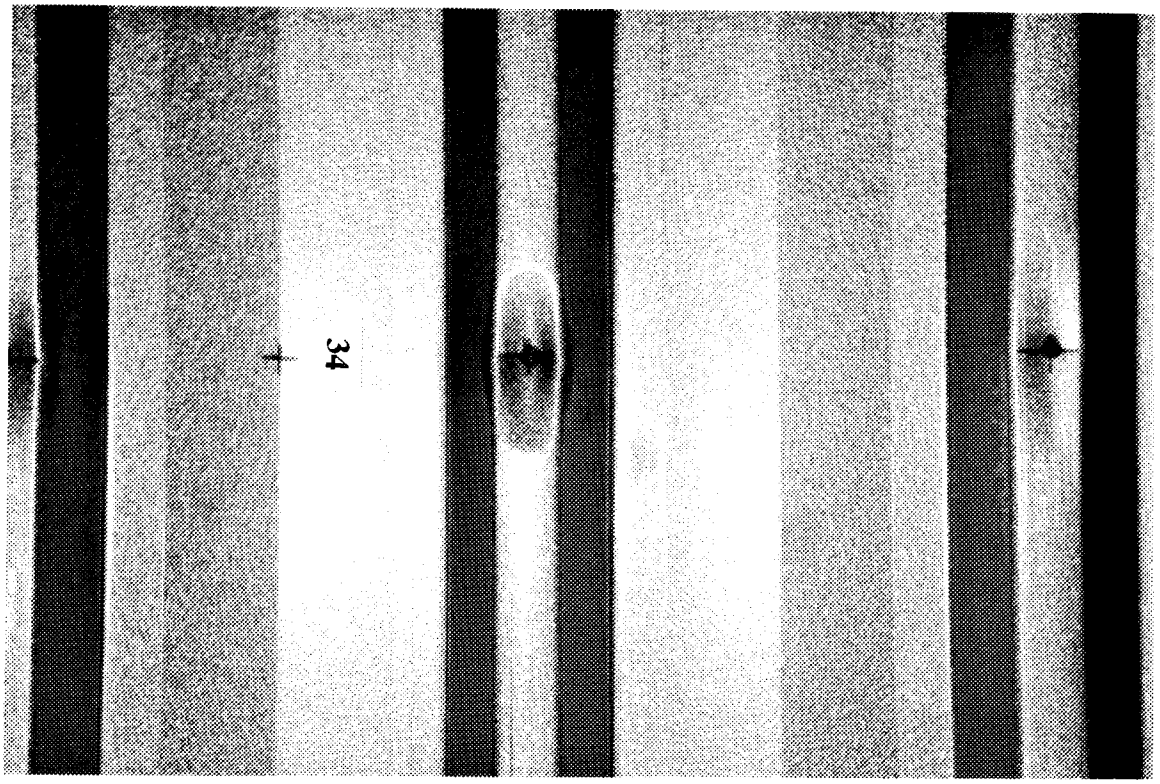

FIG. 4.13 LOCAL PLASTIC DEFORMATION OF RIBBED TYPE ROOFING SHEET

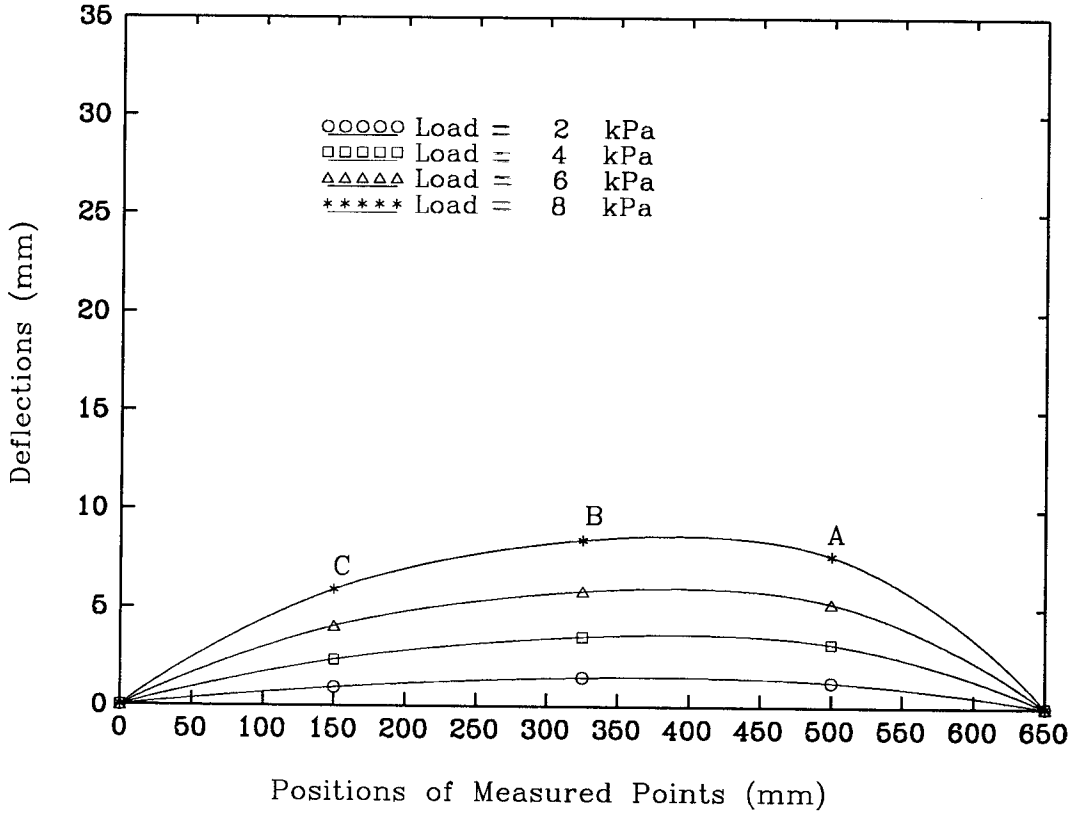

FIG.4.14 DEFLECTION OF THE SCREWED CREST IN LONGITUDINAL DIRECTION OF RIBBED TYPE ROOFING SHEET

The deflection profiles of the ribbed type roofing in longitudinal directions at different load stages are shown in Figs. 4.14. It is obvious that the overall deflection of the crests of the ribbed type roofing was much smaller than that of the other two types.

4.2 Fastener Reaction Force-Deflection Response

All two-span roofing tests showed that plastic deformation and initial failure or final failure of roofing sheets usually occurred around screw fasteners at the central support. Such localised plastic deformation and collapse were closely related to fastener reaction forces. Therefore, most commercial tests of roofing sheets are designed to directly control fastener reaction forces or so-called average load per fastener (Reardon, 1980; Mahendran, 1990). Some much simpler panel pull-over tests are also based on this local failure mode (Ellifritt and Burnette, 1990). The fastener force-deflection response curves measured in the tests, which reflected local structural behaviour, are presented in this section to compare with previous results available in the literature and provide a further discussion.

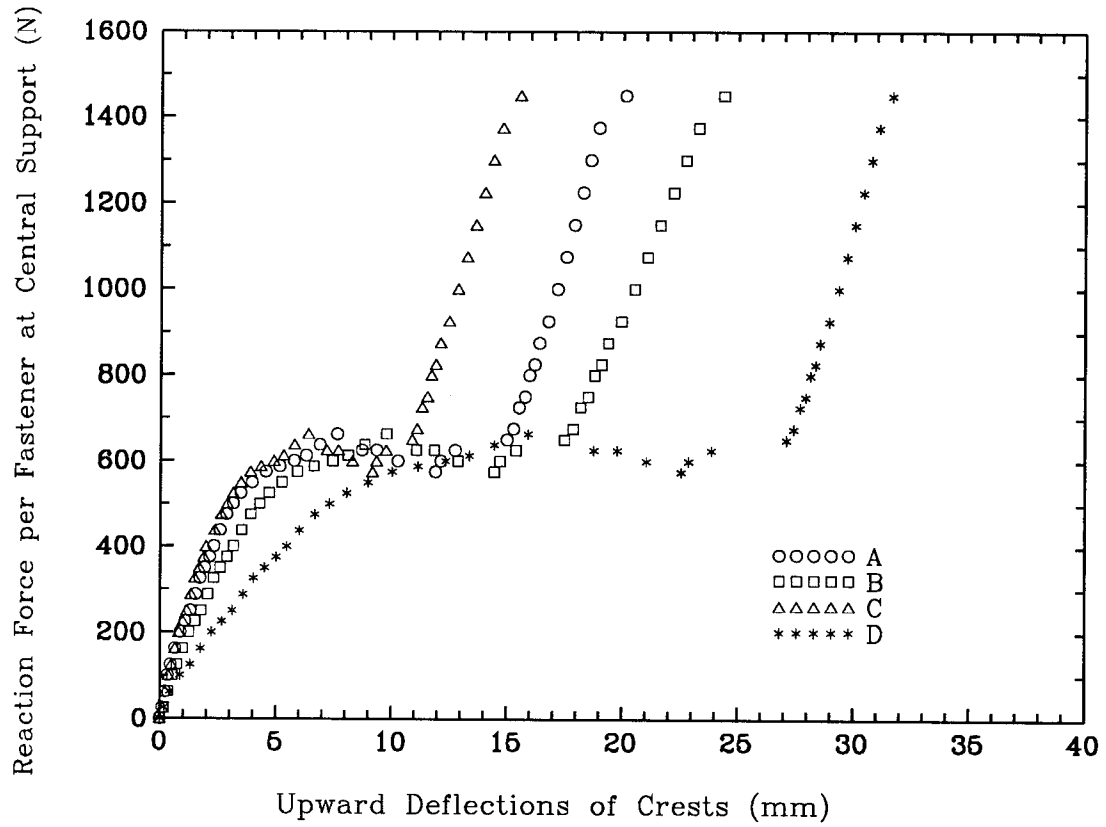

FIG.4.15 REACTION FORCE-DEFLECTION CURVES OF ARC-TANGENT TYPE ROOFING SHEET

Fig. 4.15 shows the fastener force-deflection response of the arc-tangent type roofing sheet. The measured deflection points were the same as those described in Section 4.1. The reaction force ("load") per fastener at the central support was used in the ordinate. The general trend of the fastener force-deflection curve was similar to that of the load-deflection curve shown in Fig. 4.1, but there was a small snap-through due to local buckling. Three stages, namely, the working stage, the yielding stage and the deflection hardening stage can be identified. The lower and upper limit values for the initial failure (yielding stage) were, respectively, about 580 N and 650 N per fastener. The value of 650 N per fastener was reported by Mahendran (1990) for the same span arc-tangent type roofing sheet. The repeated tests also showed the nearly same values.

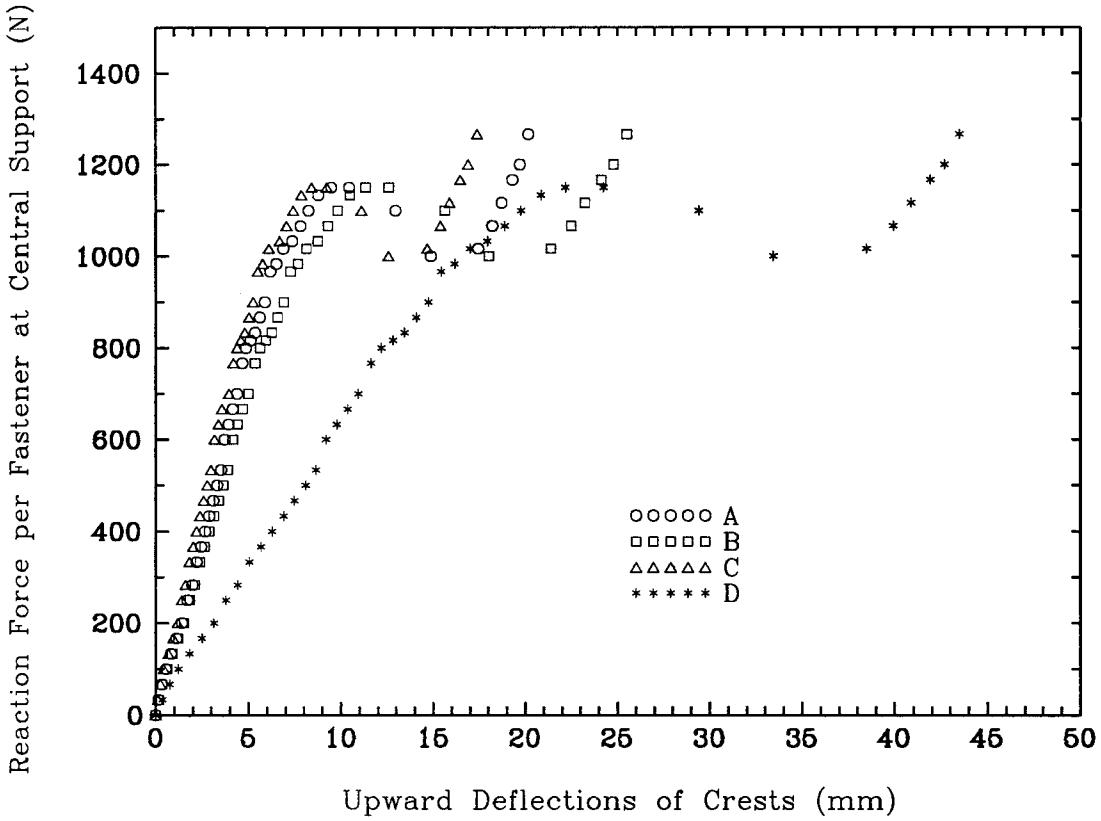

FIG.4.16 REACTION FORCE–DEFLECTION CURVES OF TRAPEZOIDAL TYPE ROOFING SHEET

The fastener force-deflection response of the trapezoidal type roofing sheet is shown in Fig. 4.16. Compared with Fig. 4.7, there was obvious difference regarding to the yielding stage. A significant snap-through phenomenon was found in the fastener force-deflection response curve rather than in the load-deflection curve. This snap-through was closely related to

local elastic-plastic large deformation and buckling around the screw fasteners, especially in the joint area between the top surface and the two sides of the screw crest at the central support. The lower and upper limit values of the initial failure (yielding stage) were, respectively, about 1000 N and 1160 N per fastener.

There was no yielding stage or deflection hardening stage in the ribbed type roofing sheet, as shown in Fig. 4.17. The relation between fastener reaction force and sheeting deflection was monotonic. The final failure was due to large local plastic strain. The ultimate value of the roofing sheet was about 1350 N per fastener. Mahendran (1988) tested a two-span similar profiled roofing of 800 mm width and 1800 mm length with five screws using an air bag method. He obtained an ultimate reaction force per fastener of 1300 N.

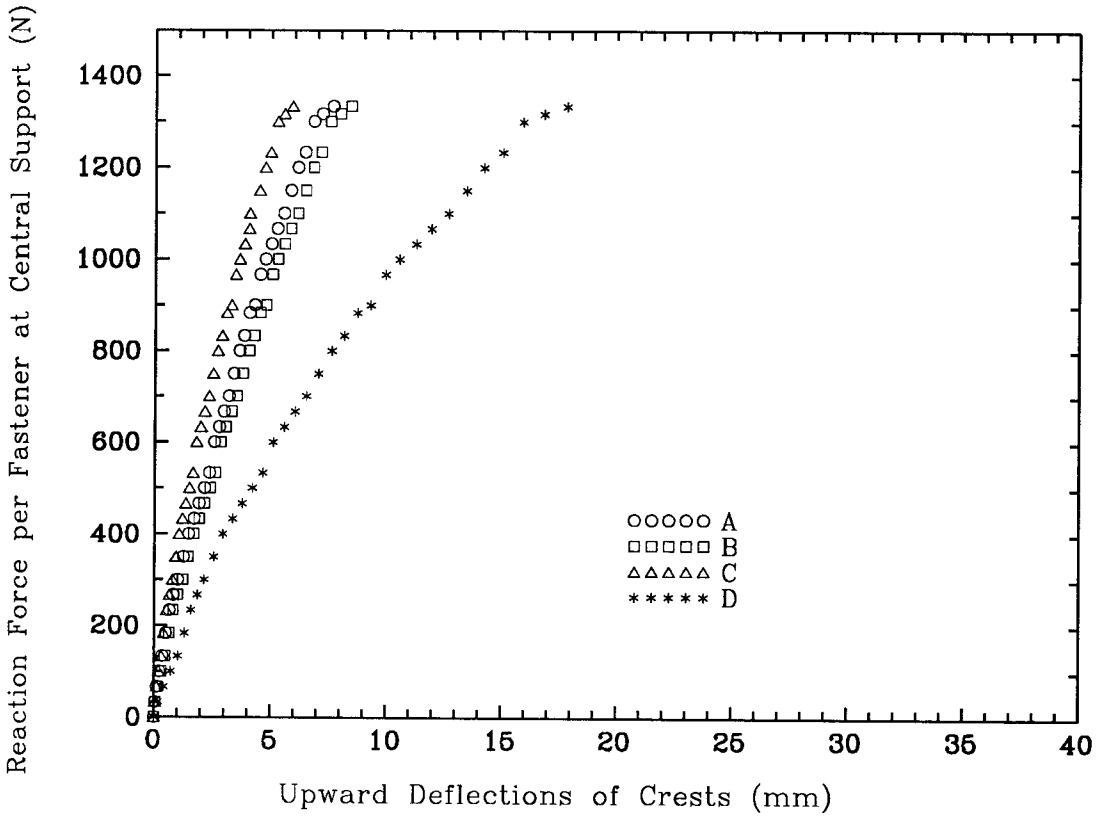

FIG.4.17 REACTION FORCE-DEFLECTION CURVES OF RIBBED TYPE ROOFING SHEET

4.3 Effect of Roof Sheeting Profile on Structural Behaviour

From the aforementioned description of experimental results of the three type roofing sheets, some general comments can be made regarding

effects of sheeting profiles on static structural behaviour of the roofing sheets under simulated wind uplift.

Fig. 4.18 shows load-deflection curves at point B for comparison between the three types of roofing sheets. Both trapezoidal and arc-tangent type roofing sheets had a yielding stage and a deflection hardening stage. This kind of characteristic was useful for preventing roofing sheets from pulling over screw fasteners during very strong short-term wind and avoiding further damage to buildings, houses and residents. The final failure of the ribbed type roofing was due to sudden cracks of the roofing sheets under the head of the screw fasteners. Therefore, its failure reliability was relatively low when subjected to one single gust of strong wind. Based on the observation of the large distortion process of the arc-tangent and trapezoidal roof sheeting profile, it was thought that the presence of unscrewed crests provided an ability to form a new stress distribution during large cross-sectional distortion of the roofing sheets so that so-called yielding and deflection hardening stages occurred. Wide pans rather than unscrewed crests in the ribbed type roof sheeting made the roof assembly lose these two stages.

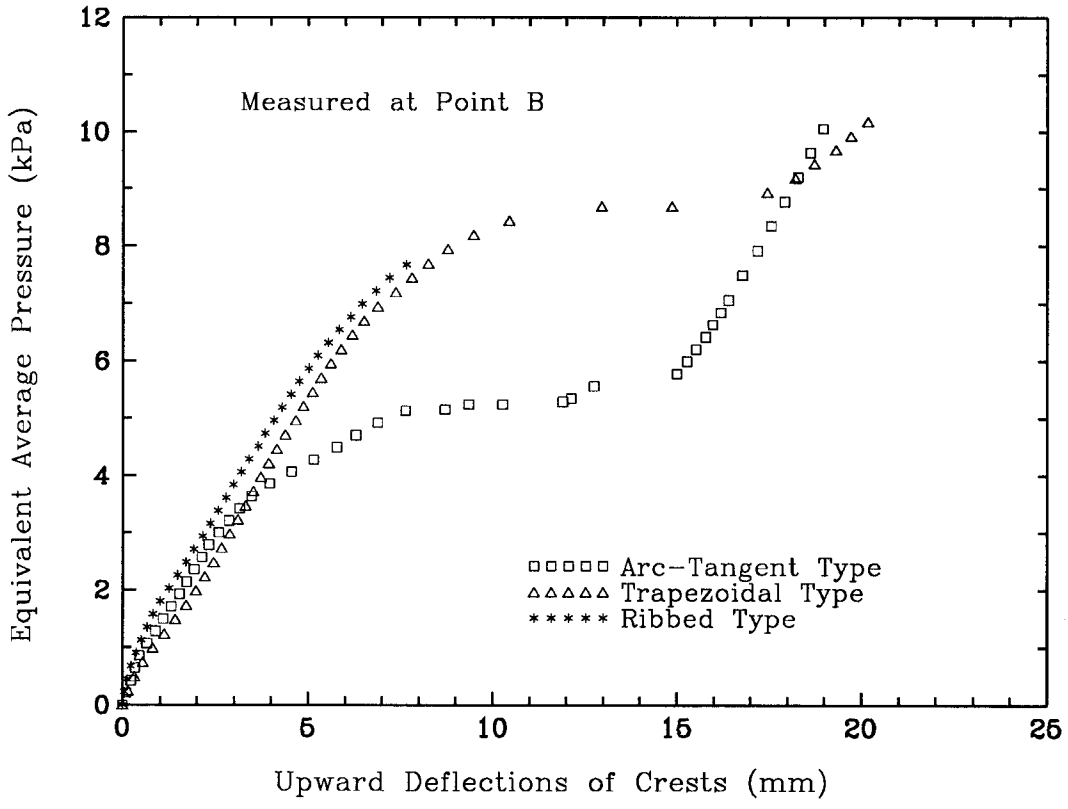

FIG.4.18 EQUIVALENT WIND PRESSURE-SHEETING DEFLECTIONS

The experimental results also showed that both ribbed and trapezoidal type roofing sheets had a higher value of limit load than arc-tangent type roofing sheets, referring to initial failure. This is probably attributed to the shape and height of screwed crests. The screwed crest shapes of both ribbed and trapezoidal type roofing sheets were similar to each other. As a results, the corresponding local deformation patterns and limit values for initial failure were similar as well. The crest shape of the arc-tangent type roofing sheet was quite different from the other roofing sheets. The measured height of the screwed crest of the arc-tangent type roofing sheet was only 17 mm on average while it was 24 mm on average for the trapezoidal type roofing sheet. As a result, there was a significant difference in limit load for initial failure between arc-tangent type roofing sheets and trapezoidal type roofing sheets.

It should be emphasised that the abovementioned structural behaviour was in response to static loading. The fatigue behaviour of light metal roofing sheets may be different from the static behaviour. However, the preliminary cyclic load tests, by using displacement-controlled method, showed that the fatigue failure of three type roofing sheets was also local, i.e., only around the screw fastener. Local fatigue did not affect the overall structural behaviour until crack propagation. Fig. 4.19 shows the hysteresis loop evolution of the arc-tangent type roofing sheet due to cyclic loading. It was obvious that crack initiation and crack propagation at the edges of fastener holes A^*, C^* and D^* did not affect the hysteresis loops of the measuring point. Until the fatigue crack was observed at the edge of fastener hole B^*, the hysteresis loop slightly became narrow and the amplitude of the loop slightly reduced.

5. EFFECT OF CYCLONE WASHERS, ROOFING SPAN AND SHEETING THICKNESS

5.1 Effect of Cyclone Washers

Although cyclone washers are usually used in cyclone prone areas to resist sustained fluctuating wind and prevent roofing sheets from fatigue failure rather than short-term strong wind, the understanding of static behaviour of roofing sheets with cyclone washers is useful for the future fatigue tests.

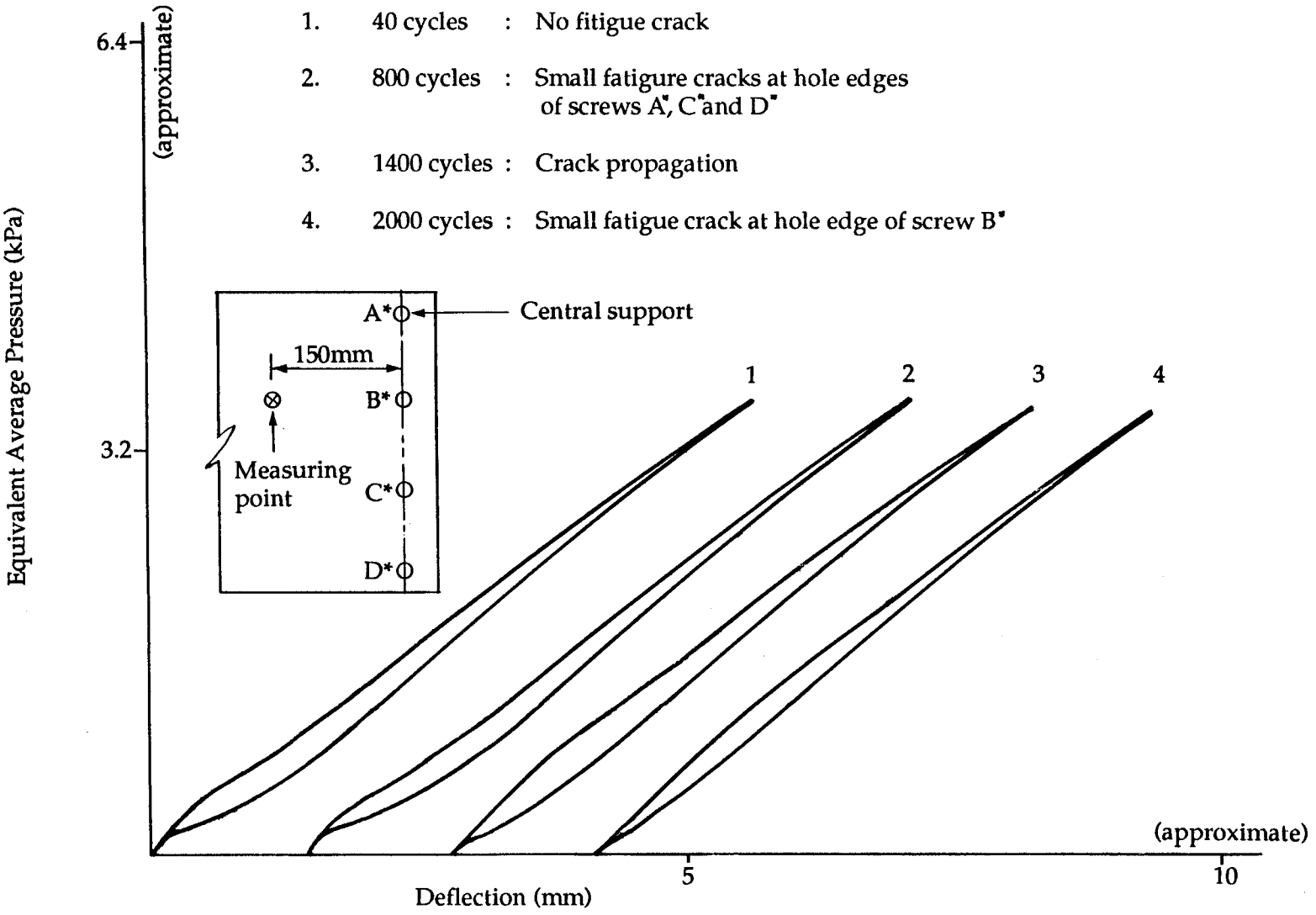

FIG. 4.19 EVOLUTION OF HYSTERESIS LOOPS OF ARC-TANGENT TYPE ROOFING SHEET DUE TO CYCLIC LOADING

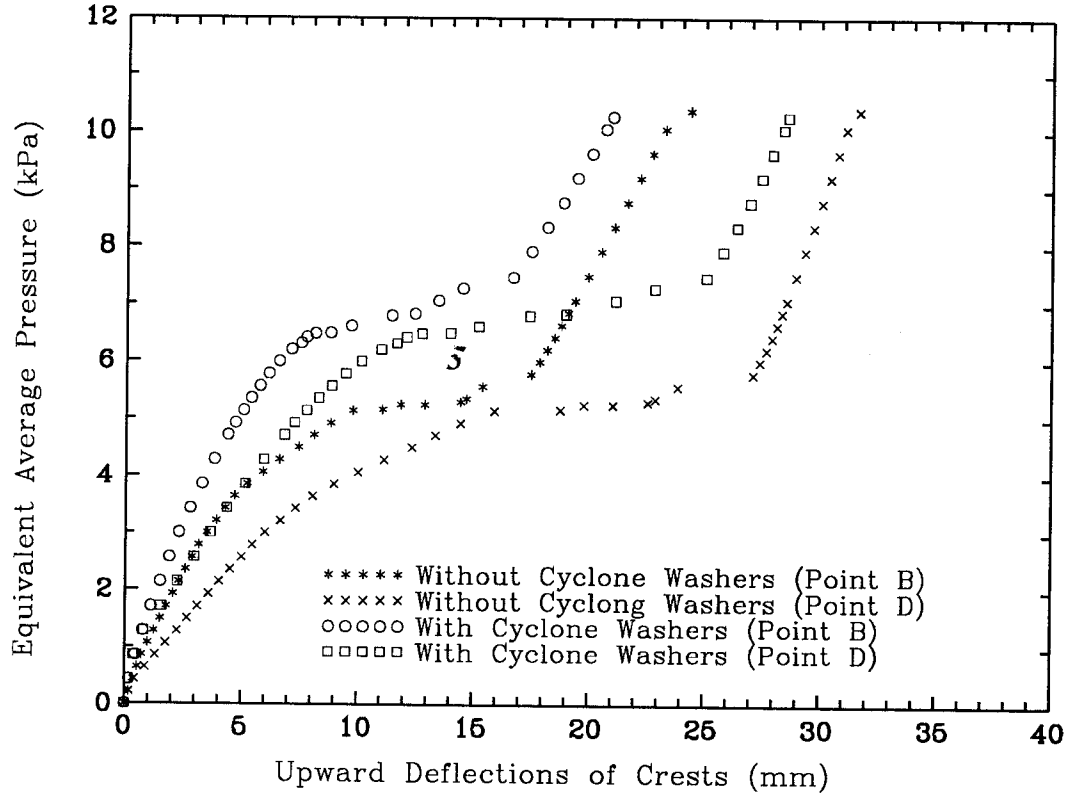

FIG.5.1 EFFECT OF CYCLONE WASHERS ON LOAD-DEFLECTION RELATION OF ARC-TANGENT TYPE ROOFING SHEET

Fig. 5.1 shows the effect of cyclone washers on load-deflection relation of the arc-tangent type roofing sheet. The experimental data were taken from measuring points B and D, as shown in Fig. 4.2. It is seen that the initial slope of the load-deflection curves with cyclone washers was steeper than that without cyclone washers. The limit value of equivalent pressure for the initial roof sheeting failure was increased to over 6.5 kPa, an increase of 30%, compared with the results without cyclone washers. As wind uplift was further increased, however, the adopted thin skin steel washers were unable to maintain restriction to the large local plastic deformations and large cross-sectional distortion. The yielding stage and deflection hardening stage still remained. Presented in Fig. 5.2 is local plastic deformation around the fastener holes with the use of cyclone washers. Compared with the case without cyclone washers, there was no obvious diamond-shape plastic deformation associated with plastic buckling. An asymmetrical vortex-type plastic deformation occurred away from the fastener holes. This fact indicates that the use of cyclone washers reduced stress concentration around the fastener holes and restrained initial cross-sectional distortion of the arc-tangent type roofing sheet so that a higher limit value for initial sheeting failure was achieved.

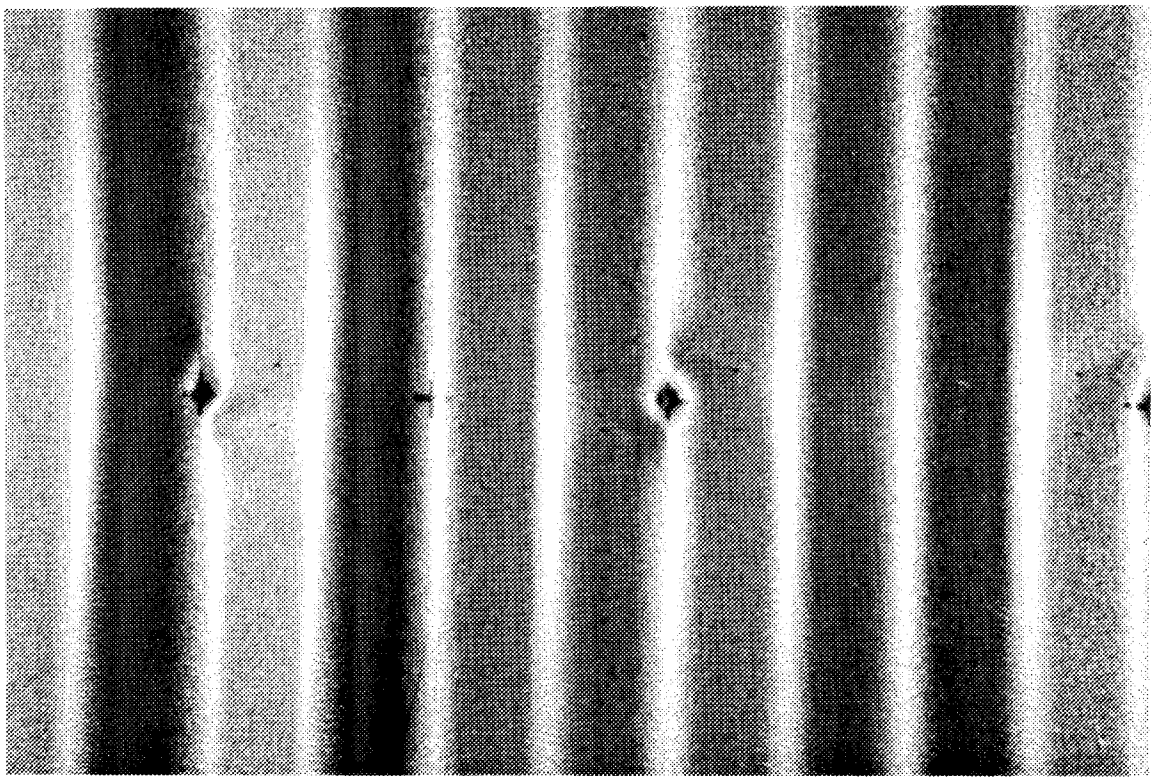

FIG.5.2 LOCAL PLASTIC DEFORMATION WITH CYCLONE WASHERS

The relation between fastener reaction force and deflection with cyclone washers is shown in Fig. 5.3 and compared with that without cyclone washers. The lower and upper limit values of reaction force per fastener for the initial failure were 870 N and 890 N, respectively, which was approximately 1.4 times as high as those values without cyclone washers. The difference between the lower and upper limit values also decreased.

Fig. 5.4 shows the effect of cyclone washers on the load-deflection relation of the trapezoidal type roofing sheet. The use of the cyclone washers raised the initial slope of load-deflection curves as in the case of the arc-tangent type roofing sheet. However, the limit value of wind uplift for the initial failure remained approximately the same as that without cyclone washers, and the cyclone washers could not resist the large cross-sectional distortion of the roofing sheet (see Fig. 5.5). As for local structural behaviour around the screw fasteners at the central support, Fig. 5.6 shows that the limit value of reaction force per fastener with cyclone washers at the central support was higher than that without cyclone washers. However, there was a much deeper snap-through, which indicates less local structural stability. The increase of the limit reaction force and the unchanged limit

wind uplift were closely related to the relation between the wind uplift and fastener reaction force. This is discussed in Section 6.1.

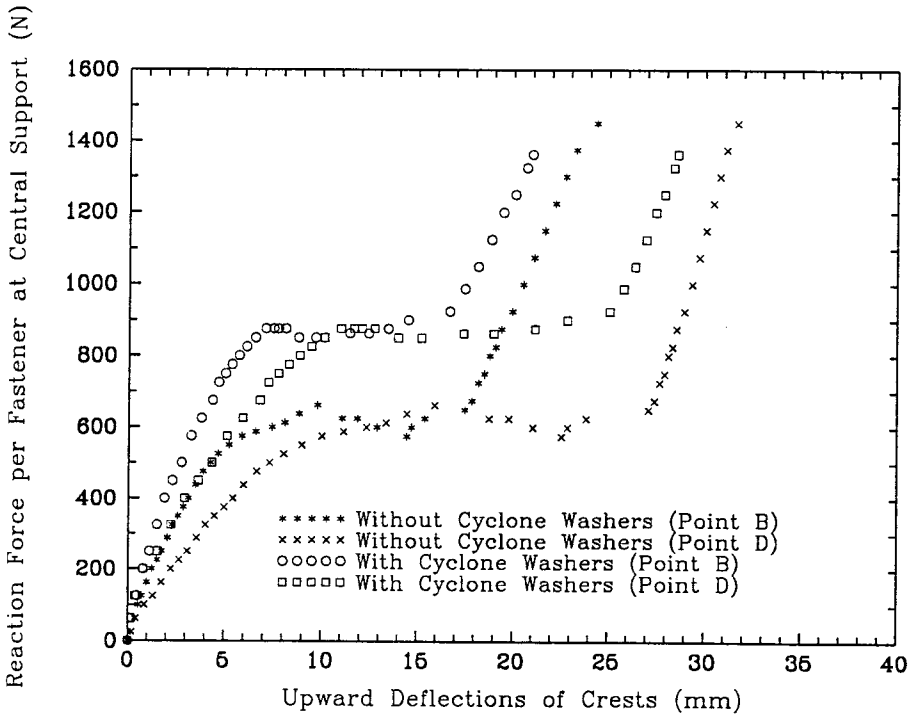

FIG.5.3 EFFECT OF CYCLONE WASHERS ON REACTION FORCE-DEFLECTION RELATION OF ARC-TANGENT TYPE ROOFING SHEET

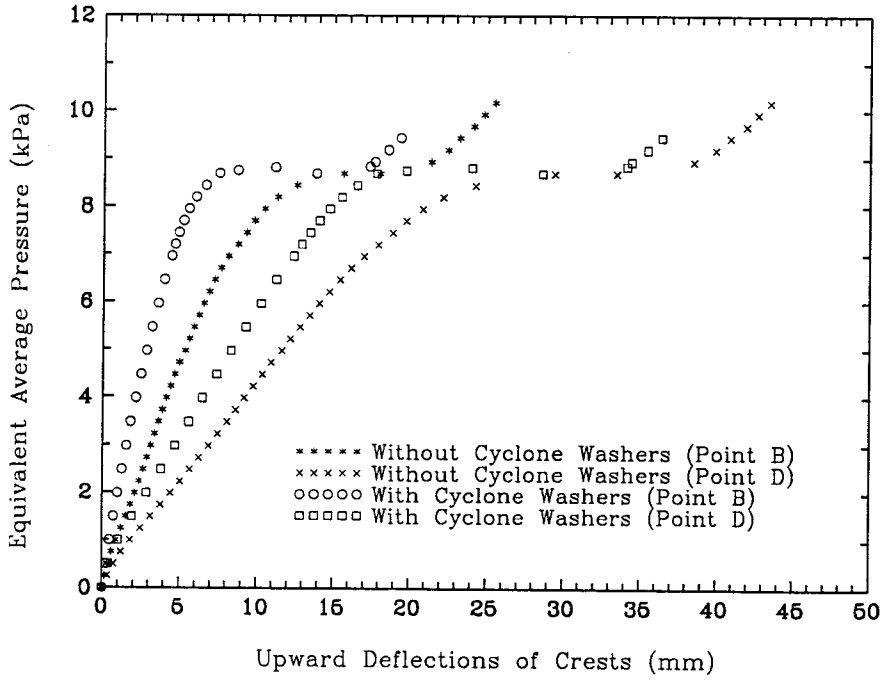

FIG.5.4 EFFECT OF CYCLONE WASHERS ON LOAD-DEFLECTION RELATION OF TRAPEZOIDAL TYPE ROOFING SHEET

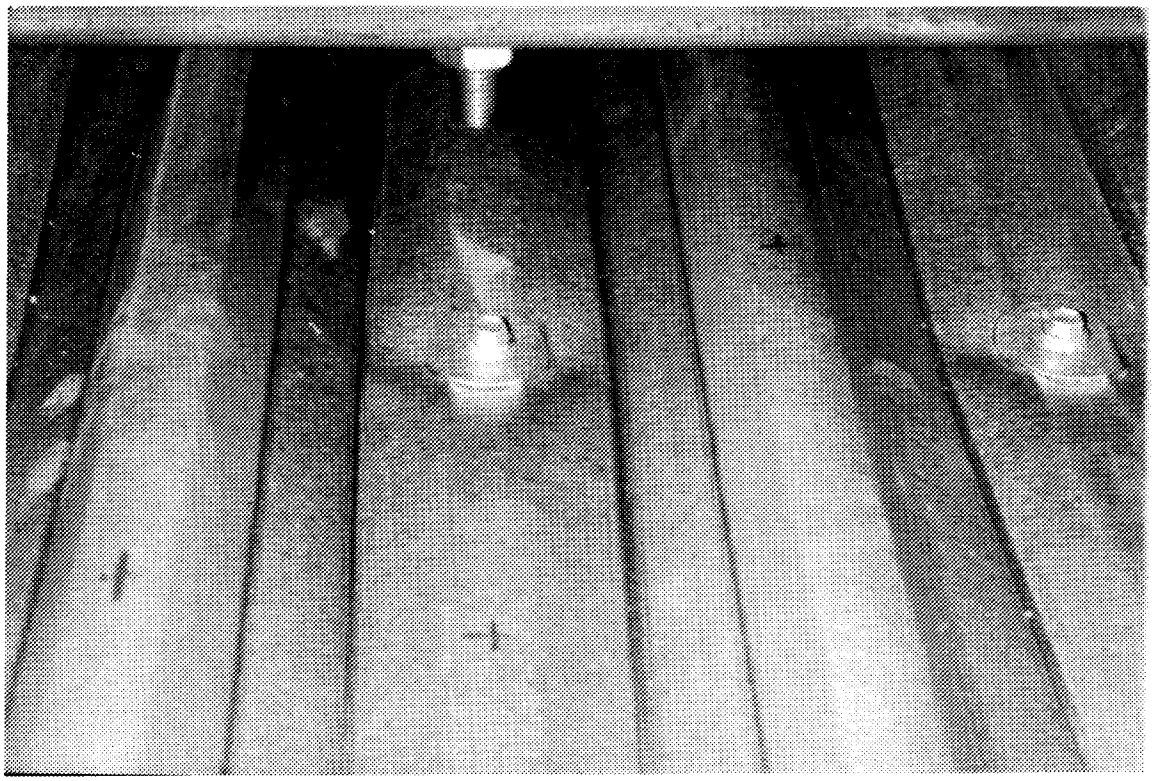

FIG. 5.5 LARGE CROSS-SECTIONAL DISTORTION OF TRAPEZOIDAL TYPE ROOFING SHEET WITH CYCLONE WASHERS

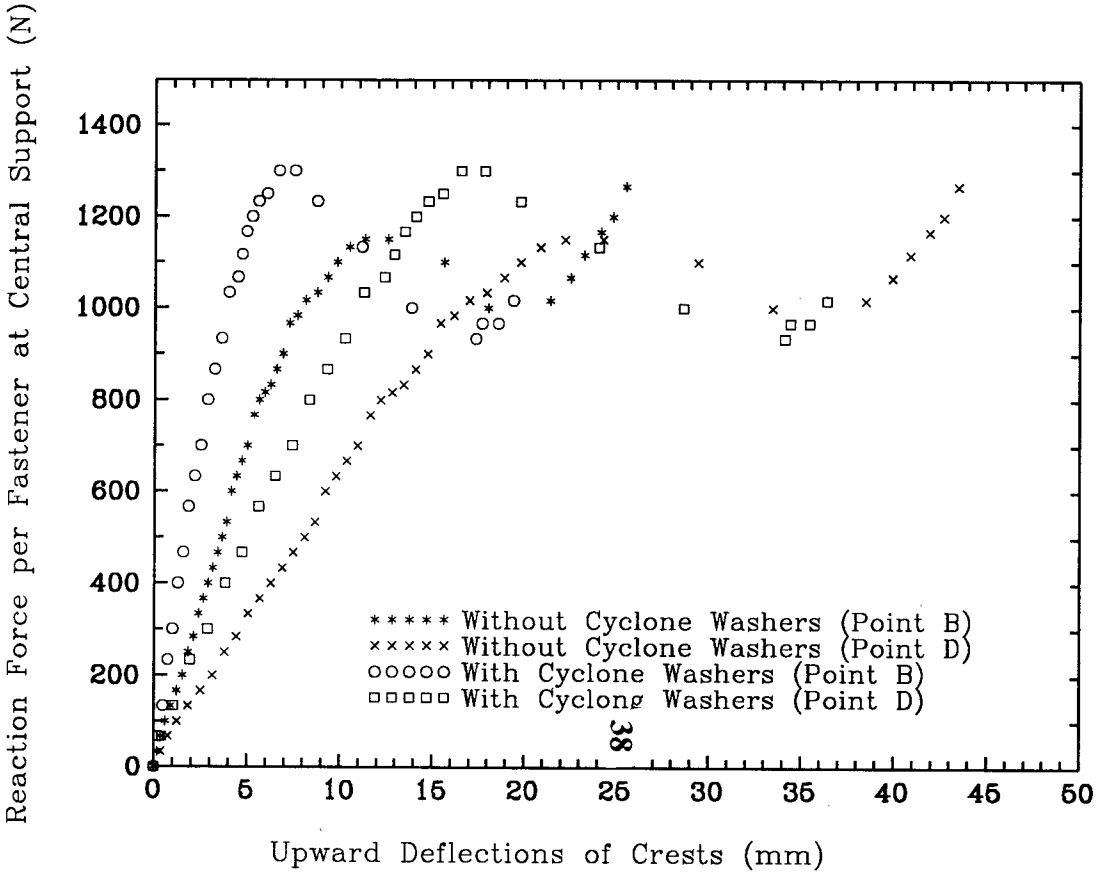

FIG.5.7 EFFECT OF CYCLONE WASHERS ON REACTION FORCE–DEFLECTION RELATION OF TRAPEZOIDAL TYPE ROOFING SHEET

The effect of the cyclone washers on the overall structural behaviour of the ribbed type roofing sheet is showed in Fig. 5.7. The slope of the load-deflection curves was again increased, which means that overall sheeting deflection was reduced under a given wind uplift. The ultimate load was increased by a factor of 1.15. Form the fastener reaction force-deflection curves the ultimate fastener reaction force at the central support was found to be increased by a factor of 1.22. The increase of ultimate load or reaction force was attributed to restriction of the local plastic deformation provided by cyclone washers. It should be pointed out that with the cyclone washers, the final failure was due to the cross-sectional crippling along the midspan load pads rather than the abrupt fracture of the plastic dimple at the central support. Therefore, the actual ultimate values were probably higher than the abovementioned values. Nevertheless, this increase might not be significant because at that stage, buckles were also observed around the screwed fastener at the central support.

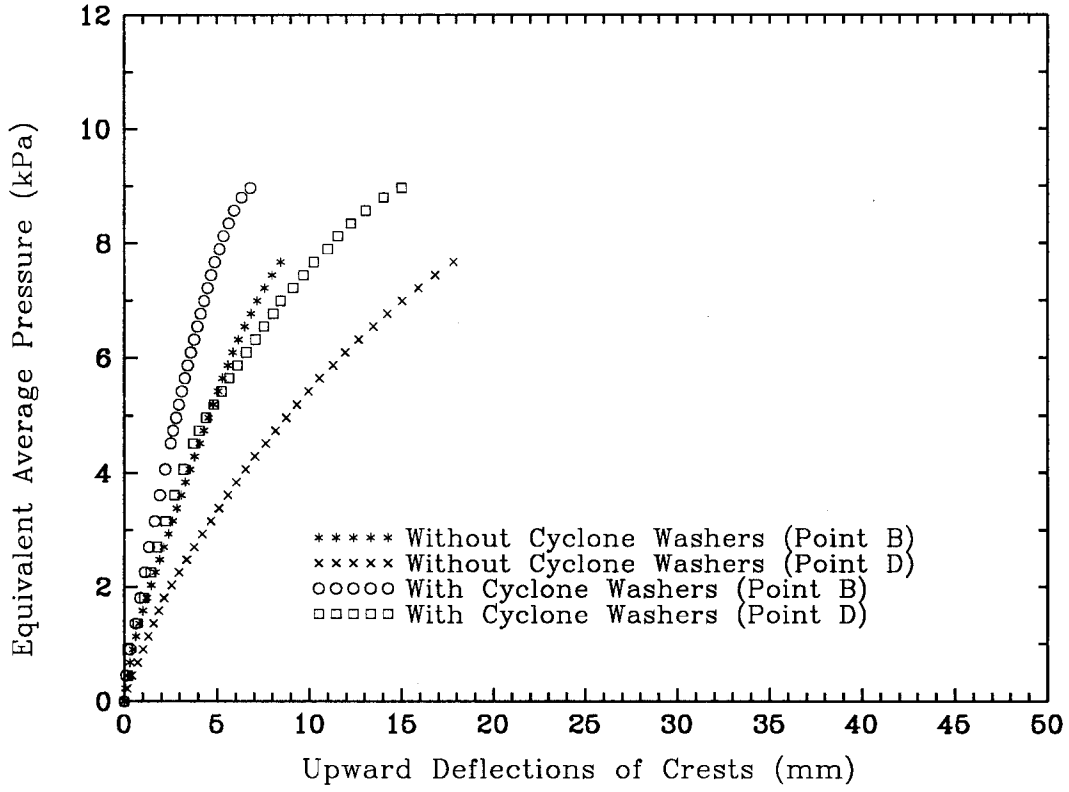

FIG.5.7 EFFECT OF CYCLONE WASHERS ON LOAD-DEFLECTION RELATION OF RIBBED TYPE ROOFING SHEET

From the above discussion, it can be seen that the use of cyclone washers can raise the initial slope of load-deflection curves, reduce the roof sheeting deflection before the initial failure, and more and less, increase the

limit values of load or fastener reaction force. The fact that the use of the cyclone washers was more effective for the arc-tangent roofing sheet than the other two types also indicated a necessity of studying shape, stiffness and size of cyclone washers relative to roofing shape, stiffness and size. This can be achieved only after the stress field around the screw fastener at the central support is determined. It should be pointed out that the results and suggestions only refer to the static behaviour of the roofing sheet.

5.2 Effect of Roofing Span

There are varieties of roofing spans in practice. Only two kinds of roofing spans of 900 mm and 1200 mm were included in this investigation. The experimental results of the equivalent 900 mm span (650 mm in the test) roofing sheets have been introduced before. The results of the equivalent 1200 mm span (870 mm in the test) roofing sheets are presented and compared with the results of the equivalent 900 mm span roofing sheets in this section.

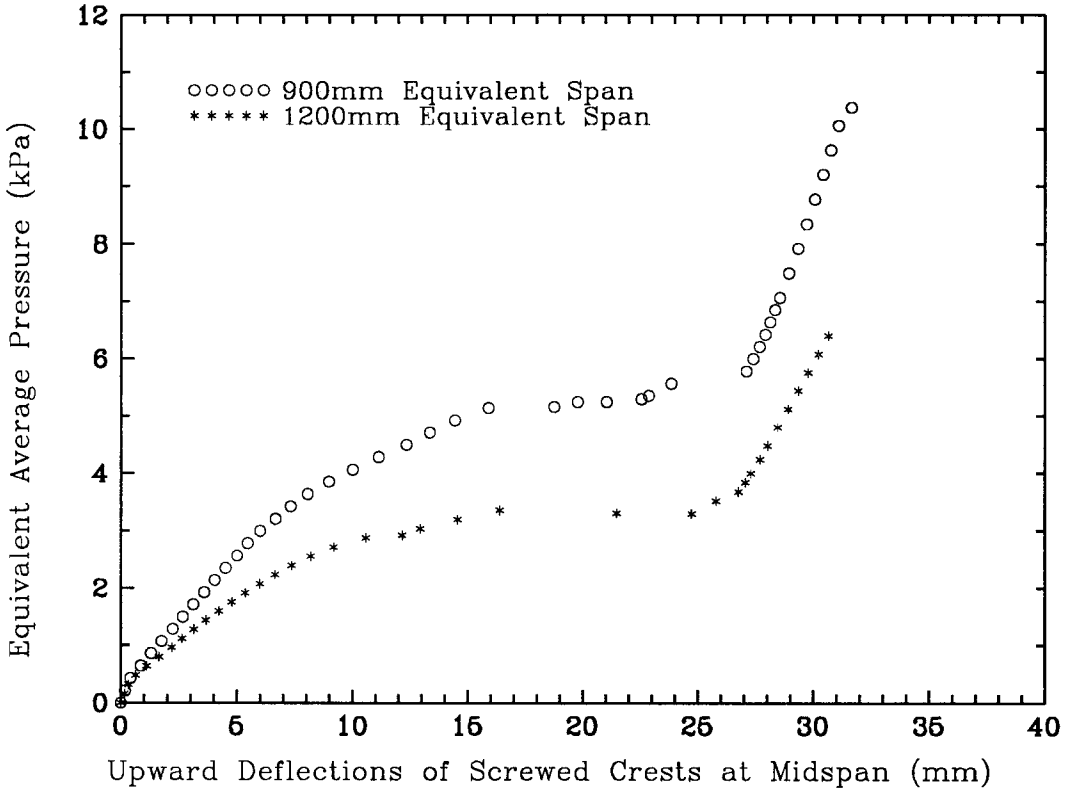

FIG.5.8 EFFECT OF ROOFING SPANS ON LOAD-DEFLECTION RELATION OF ARC-TANGENT TYPE ROOFING SHEET

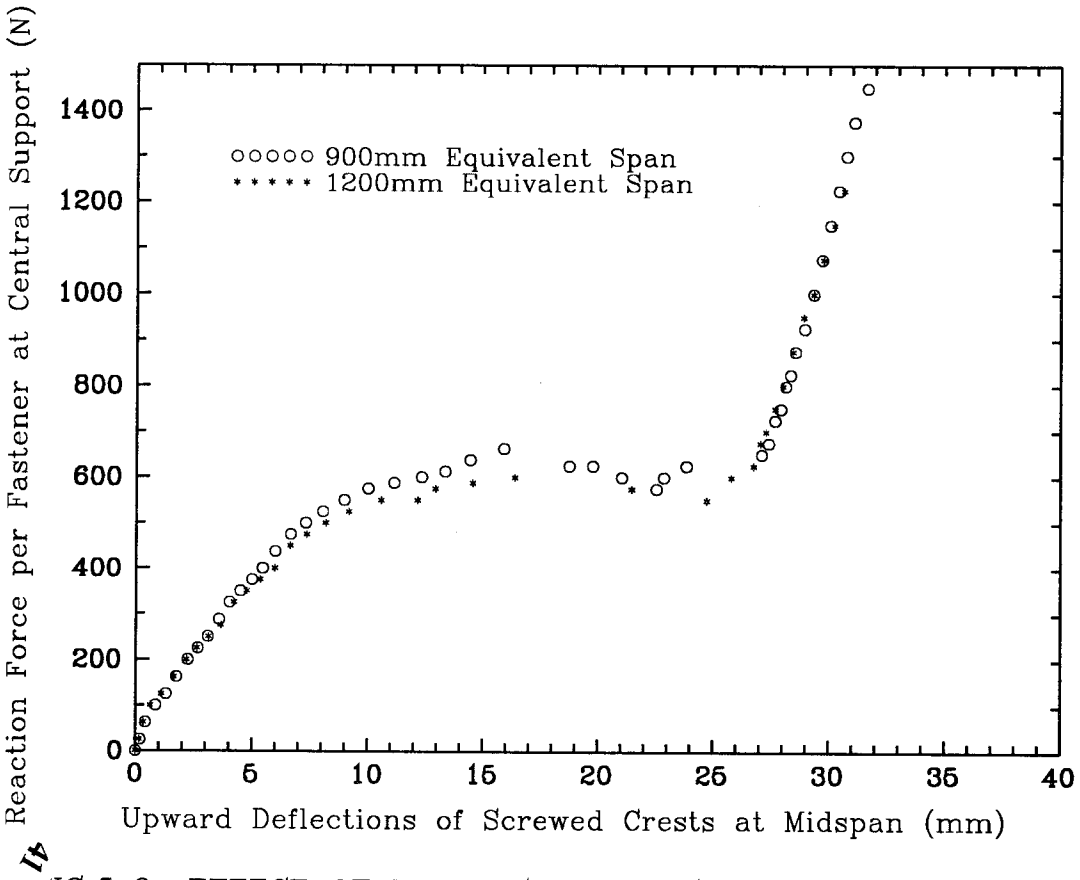

FIG.5.9 EFFECT OF ROOFING ON REACTION FORCE-DEFLECTION RELATION OF ARC-TANGENT TYPE ROOFING SHEET

From the previous description, it is known that either initial failure or final failure of roofing sheets was due to local yielding or local buckling around the screw fasteners at the central support. Therefore, the effect of roofing spans on ultimate wind pressure would be much larger than the effect on ultimate fastener reaction force. This is because load-deflection curves reflect an overall structural behaviour while fastener reaction force-deflection curves indicate a local structural behaviour. Fig. 5.8 shows that for the arc-tangent type roofing sheet, the limit value of equivalent pressure for the initial failure was only about 3.2 kPa for the long span (1200 mm) roofing while the corresponding value for the 900 mm span roofing was about 5 kPa. Nevertheless, the limit value of reaction force per fastener for the long span roofing reduced only about 6% (see Fig. 5.9). It is also seen from Figs. 5.8 and 5.9 that the structural behaviour of the long span roofing was similar to the 900 mm span roofing. In both figures, the plotted deflections were measured on the screwed crest at the midspan. It is also clear that due to the long span, the initial total roof sheeting stiffness was greatly reduced. However, local stiffness around central fasteners was not changed much, as shown in Fig. 5.9.

For the trapezoidal type roofing sheet, the difference of the limit pressure values between the equivalent 1200 mm and 900 mm span roofing sheets was quite large for the initial failure as shown in Fig. 5.10. The value corresponding to the long span roofing was about 5.5 kPa while the value for the shorter span was 8.6 kPa. It is noted that the ratio of the limit pressure values (8.6 kPa divided by 5.5 kPa) was larger than the ratio of the roofing spans (1200 mm divided by 900 mm), which means that the roofing system at this stage was nonlinear and the simple beam theory can not predict this nonlinear shell problem. There was also 15% difference of the upper limit reaction force per fastener between the roofing sheets of different spans.

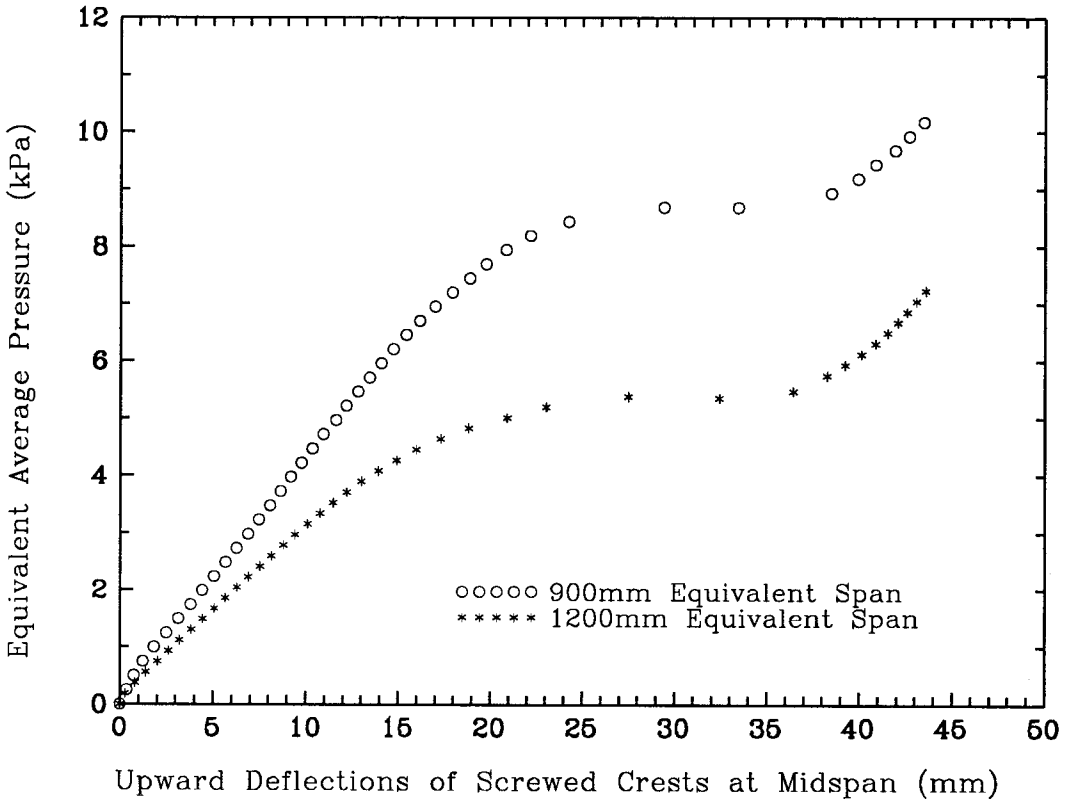

FIG.5.10 EFFECT OF ROOFING SPANS ON LOAD-DEFLECTION RELATION OF TRAPEZOIDAL TYPE ROOFING SHEET

Similar difference between the ultimate values was also found in the ribbed type roofing sheet, as shown in Fig. 5.11. The ultimate pressure value for the long span roofing sheet was about 4.8 kPa while the value for the equivalent 900 mm span roofing sheet was 7.6 kPa. The ultimate fastener reaction force was about 1180 N per fastener on average rather than 1350 N per fastener in the case of the equivalent 900 mm span roofing sheet. However, the ultimate pressure values for the long span roofing may be higher in the prototype because the final failure of the long span roofing

sheet was due to overall buckling around the midspan pads rather than the abrupt fracture observed in the equivalent 900 mm span roofing. It is obvious from Fig. 5.11 that the deflection curves of the points B and D in the long span roofing nearly overlapped. Therefore, one can say that the cross-sectional distortion of the 1200 mm equivalent span roofing sheet was much smaller than that of the 900 mm equivalent span roofing sheet.

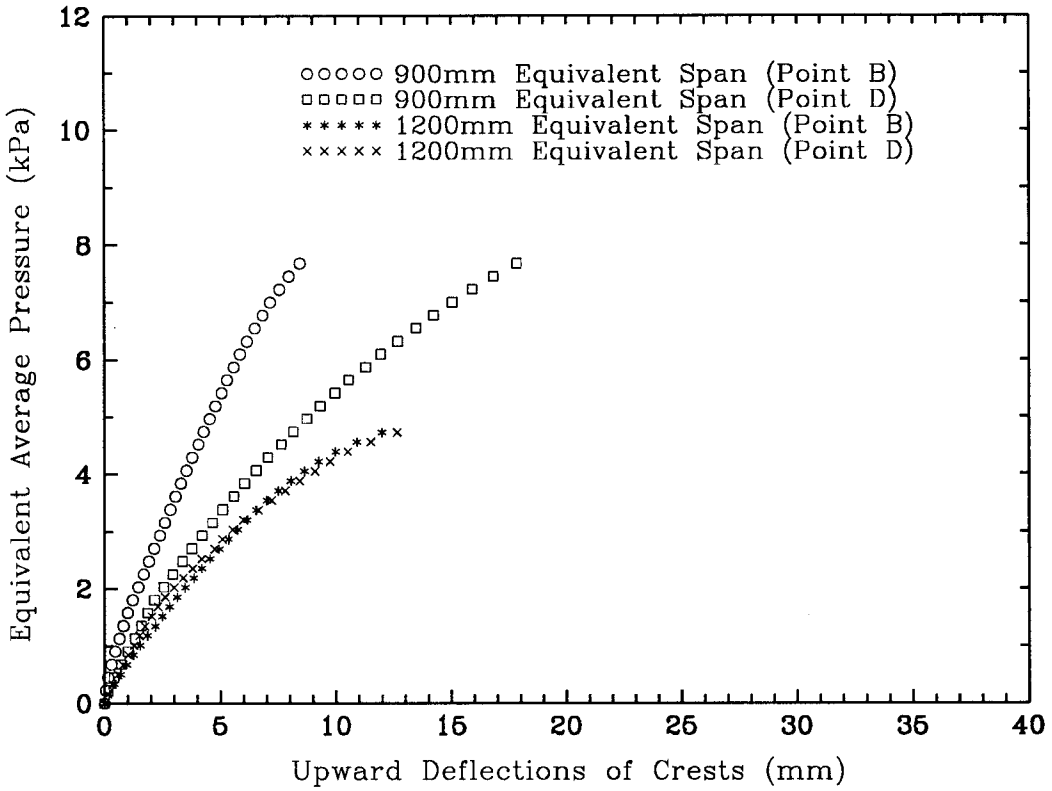

FIG.5.11 EFFECT OF ROOFING SPANS ON LOAD-DEFLECTION RELATION OF RIBBED TYPE ROOFING SHEET

It is clear from the above discussion that for the different span roofing assemblies, the reaction force per fastener had a relatively stable limit value for the initial failure of the arc-tangent and trapezoidal type roofing sheets and the ultimate strength of the ribbed type roofing sheet. This reflects the local failure characteristic of the roofing sheets. With the increase of the roofing span, however, the allowable wind pressure should be decreased. In general, the deflection behaviour and failure mode of the equivalent 1200 mm span roofing sheets were similar to those of the equivalent 900 mm span roofing sheets.

5.3 Effect of Sheeting Thickness

There are two different of sheeting thickness available for Lysaght

SPANDEK roofing sheets, i.e., 0.47 mm and 0.53 mm (TCT). A static test was also conducted on 0.53 mm thick SPANDEK roofing sheet to compare with 0.47 mm SPANDEK roofing sheet. The equivalent roofing span was still 900 mm.

Fig. 5.12 shows the comparison of load-deflection curves measured at the midspan screwed crest. The overall deflection trends were similar to each other. For the thicker roofing sheet, after the initial yielding there was an obvious snap-through related to the overall structural behaviour, which indicated that the interaction between local yielding and overall structural behaviour became stronger. The increase of sheeting thickness significantly enhanced the limit value for the initial failure of the roofing sheet. The limit value of the equivalent wind pressure increased from 8.6 kPa to 11 kPa, and the limit value of reaction force per fastener increased from 1160 N to 1550 N. Corresponding to the larger fastener reaction force, the local plastic dimple at the screwed crest of the central support was larger than that in the 0.47 mm thick roofing sheet. As a result, final failure was due to a sudden split of the bottom surface of the dimple in the transverse direction of the roofing sheet.

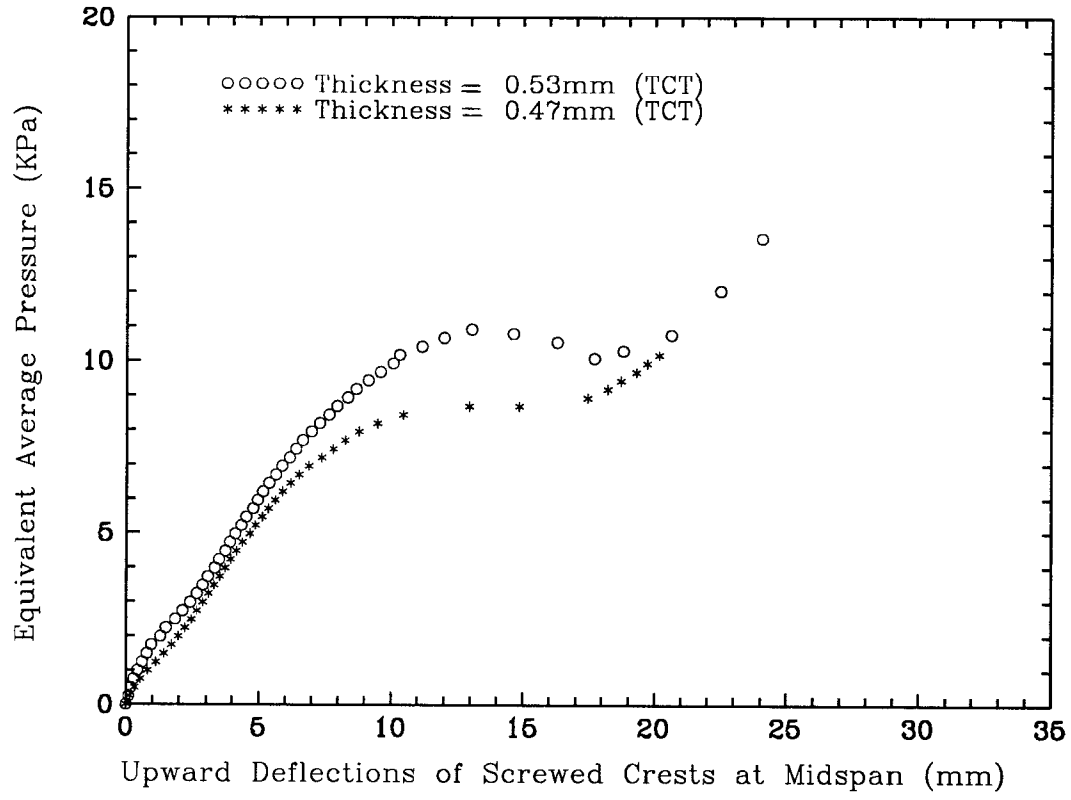

FIG.5.12 EFFECT OF SHEETING THICKNESS ON LOAD-DEFLECTION RELATION OF TRAPEZOIDAL TYPE ROOFING SHEET

Another comparison as to effects of sheeting thickness was conducted between Lysaght CUSTOM BLUE ORB roofing sheet of 0.66 mm (TCT) and Lysaght CUSTOM ORB sheet of 0.47 mm (TCT). Both sheets are made from zincalume steel, but BLUE ORB sheeting material is more ductile, with a yield stress of 300 MPa.

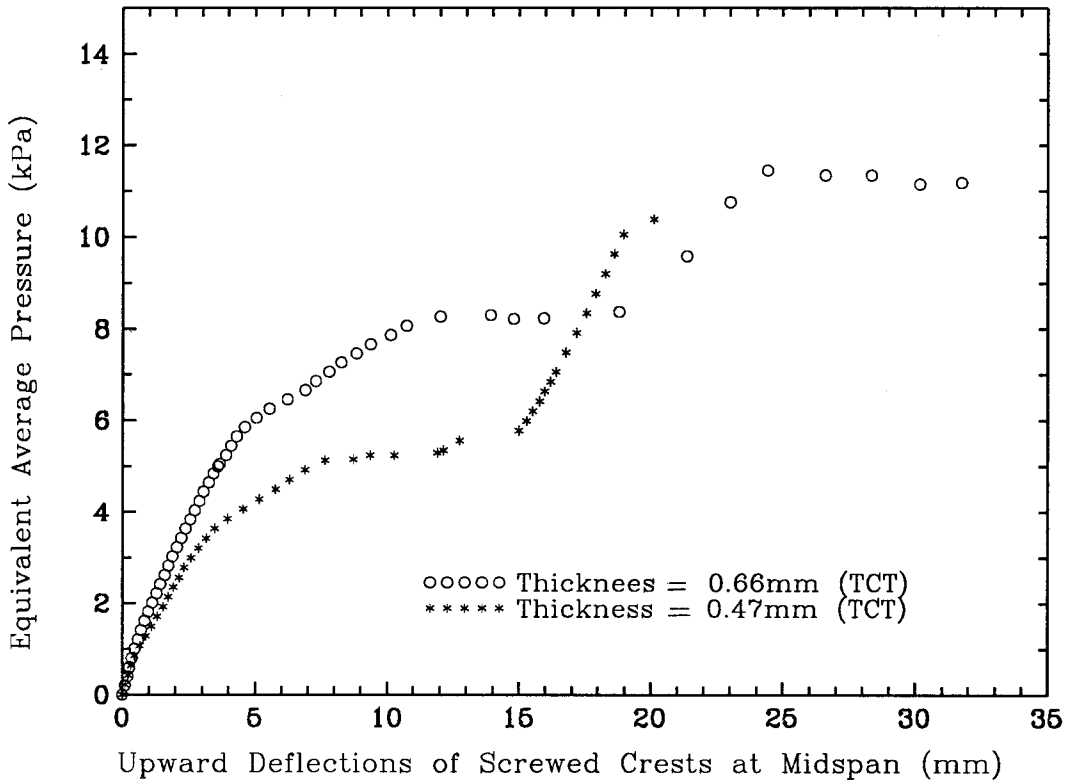

FIG.5.13 EFFECT OF SHEETING THICKNESS ON LOAD-DEFLECTION RELATION OF ARC-TANGENT TYPE ROOFING SHEET

Fig. 5.13 shows the comparison of load-deflection curves measured at the midspan screwed crests. For the BLUE ORB sheet, there were two stages of sheeting deflection before a large cross-sectional distortion developed. The first was an approximately linear relationship between pressure and deflection until a local diamond shape deformation was observed around the screw fastener at the central support. The second was the development of the local deformation. The developing process of the local deformation was plastic and gradual without buckling sound. As a result, the slope of the load-deflection curve was much lower than the first stage, but remained approximately constant until the large cross-sectional distortion occurred. The limit value of the equivalent pressure for the initial failure, which corresponded to the horizontal line, was 8.1 kPa. The corresponding value for the CUSTOM ORB sheet was 5 kPa. The lower and

upper limit values of the reaction force per fastener were 1000 N and 1120 N, respectively, for the CUSTOM BLUE ORB sheet; 580 N and 650 N for the CUSTOM ORB sheet. However, if one only considered the first approximate linear stage, the limit value was 5.8 kPa for the equivalent pressure and 900 N for the reaction force per fastener in the case of CUSTOM BLUE ORB roofing sheet.

6. DISCUSSION OF MIDSPAN LOAD METHOD

Using the midspan load method to test roofing sheets is relatively easy and economical. The local failure characteristic of roofing sheets, which was closely related to fastener reaction force, also indicated that this simplification is reasonable. However, it is not clear whether or not the assumption of the two-span continuous simply supported beam can provide the required equivalent span length and line load magnitude since real fastener assemblies are complicated and fastener arrangement is not uniformly distributed. In this investigation, wind uplift and fastener reaction force were simultaneously measured. This simple support assumption can be partly examined.

6.1 Wind Uplift-Fastener Reaction Force

Fig. 6.1 shows the relationship between the wind uplift and the fastener reaction force at the central support for the arc-tangent type roofing sheet. It included three cases: 900 mm equivalent span roofing without cyclone washers; 900 mm equivalent span roofing with cyclone washers; and 1200 mm equivalent span roofing without cyclone washers. The load-fastener reaction force relationship based on the two-span continuous simply supported beam assumption was also plotted in Fig. 6.1. In addition, the case in which the central support was a pin hinge without capacity to undergo bending moments was considered, and the corresponding load-fastener reaction force relation was plotted for comparison.

It was found that when wind uplift was small, the relation between fastener reaction force and wind uplift was approximately linear, and the two-span continuous simply supported beam assumption provided a satisfying results. When wind uplift was increased to cause a large cross-sectional distortion at the central support, the fastener reaction forces dropped. This corresponded to the approximate horizontal lines in the load-deflection curves (or reaction force-deflection curves) mentioned in previous sections. When roofing sheets restored their stiffness, the linear relation between wind uplift

and reaction force appeared and again followed the two-span continuous simply supported beam assumption. These observations were identical to the considered three cases. Therefore, the adopted assumption seems to be reasonable for the arc-tangent type roofing, except for the large cross-sectional distortion stage. In the current design procedure for roofing sheets, the limit value of "load" per fastener was first measured through roofing tests. Then the allowable wind pressure was calculated based on two span simple beam theory. Therefore, this design procedure usually provides a conservative value for the allowable wind pressure, especially at the large cross-sectional distortion stage of roofing sheets.

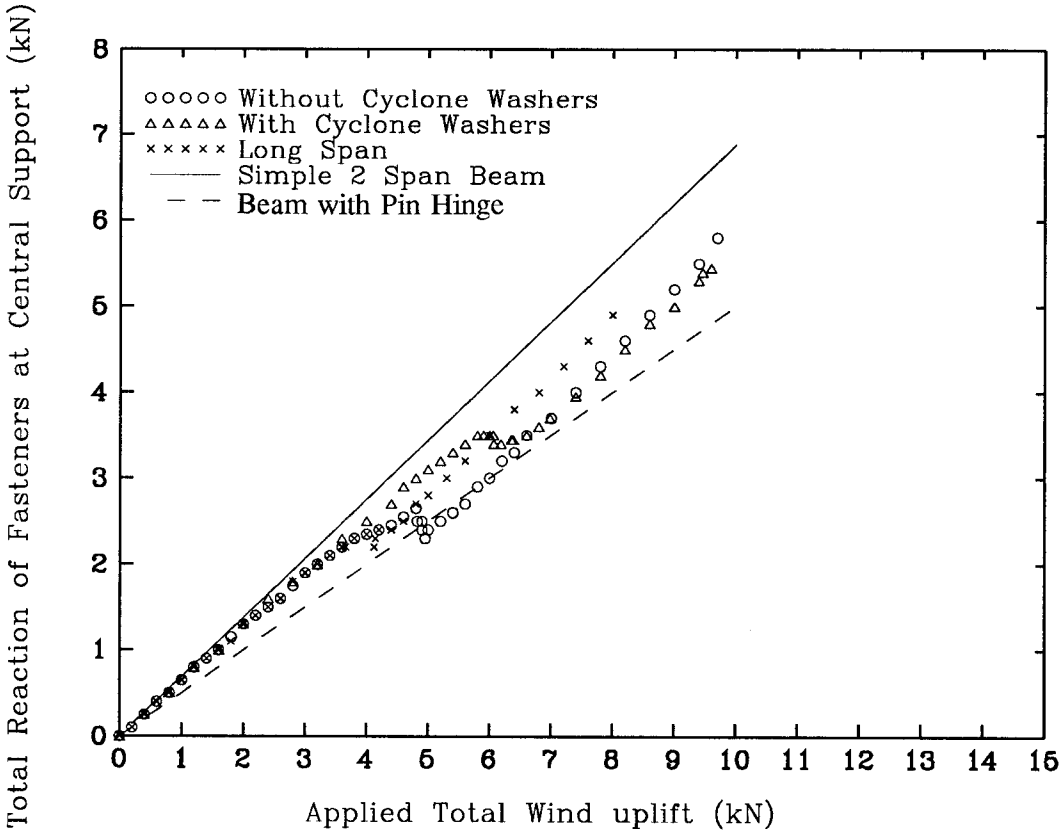

FIG. 6.1 RELATIONSHIP BETWEEN WIND UPLIFT AND FASTENER REACTION FORCE FOR ARC-TANGENT TYPE ROOFING SHEET

For the trapezoidal type roofing sheets, the two span continuous simply supported beam assumption did not fit the experimental data well (see Fig. 6.2). The measured curves departed from the solid line and approached to the dash line. This was probably associated with the earlier formation of local plastic dimple around the screw fasteners at the central support. However, relatively speaking, the long span roofing and the roofing with cyclone washers exhibited an better approach to the solid line. This is related to the stronger restraints provided by cyclone washers or the smaller local

deformation in the long span case. It is also interesting to see that there was a larger drop of the reaction force when the roofing sheet experienced a large cross-sectional distortion. The reaction force drop crossed the dash line, which means the roofing cross section at the central support experienced a process without any bending moments. The large reaction force drop made the reaction force-deflection curves exhibited a snap through, as discussed before.

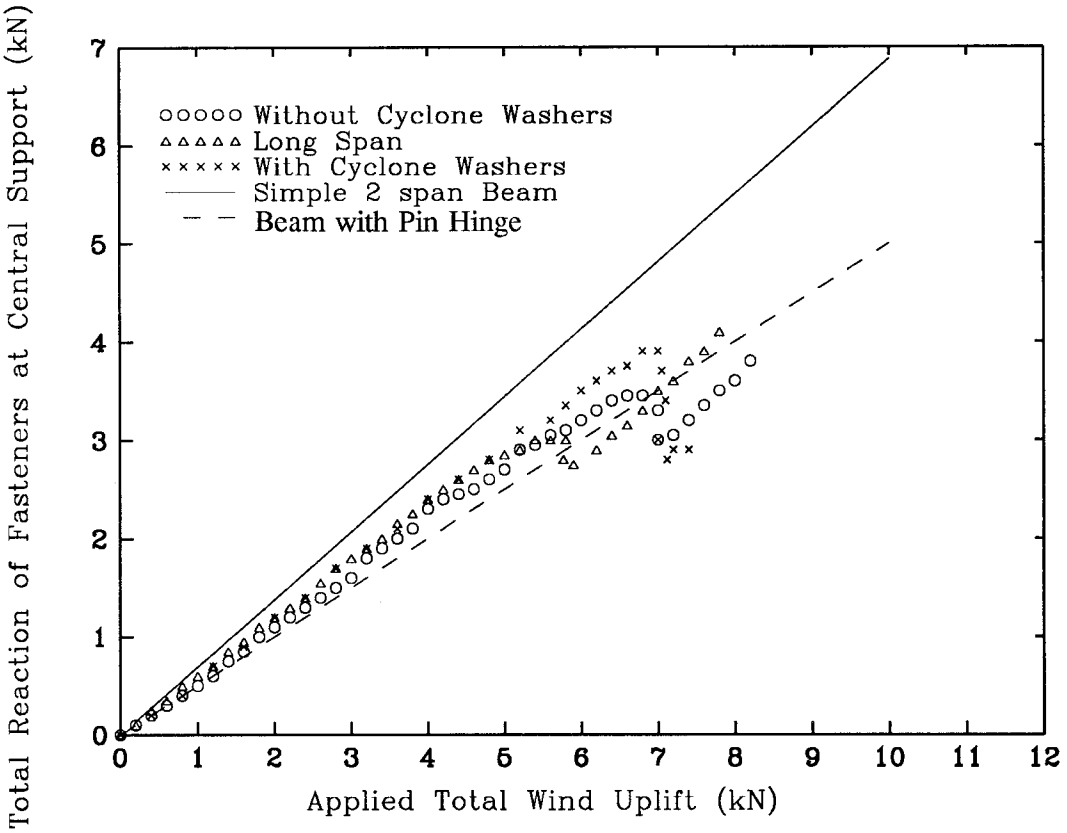

FIG. 6.2 RELATIONSHIP BETWEEN WIND UPLIFT AND FASTENER REACTION FORCE FOR TRAPEZOIDAL TYPE ROOFING SHEET

The wind uplift-fastener reaction force relation of the ribbed type roofing sheets was relatively simple (see Fig. 6.3). Such relation remained approximately linear during the whole test. In the case of the long span roofing and the roofing with cyclone washers, the two span continuous simply supported beam assumption can provide a reasonable approach to the experimental data. For the 900 mm equivalent span roofing without cyclone washers, such approach may need to be modified.

In summary, the two-span continuous simply supported beam assumption is reasonable in most cases. However, during the large cross-sectional distortion or large local plastic deformation, such an assumption is

not satisfactory. The cyclone washer reduced local plastic deformation, and the long span roofing sometimes had a relatively small local plastic deformation so that the assumption was more suitable for these cases.

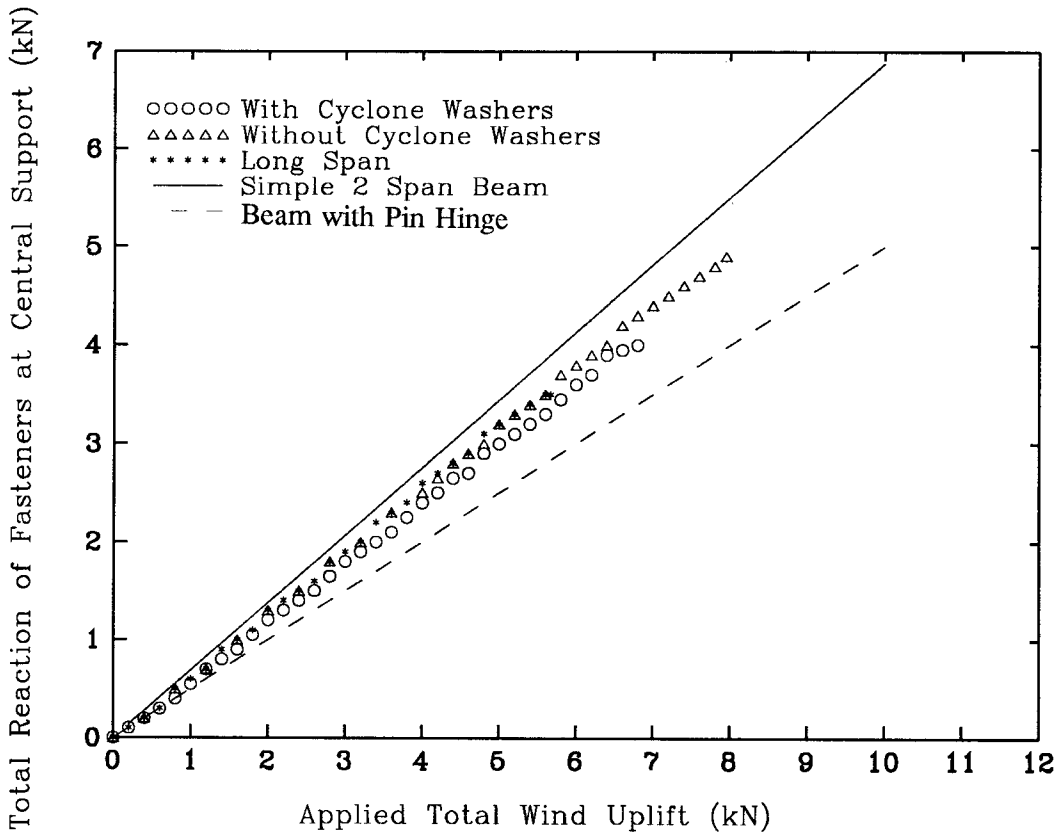

FIG. 6.3 RELATIONSHIP BETWEEN WIND UPLIFT AND FASTENER REACTION FORCE FOR RIBBED TYPE ROOFING SHEET

6.2 Midspan Loading Pads

In the midspan load method, the other phase of the basic requirement is to transmit loads exerted by midspan loading pads to fasteners at the central support in a realistic fashion. This represents a difficult problem because light gauge metal roofing sheets often have a complex profile. To simulate line distributed wind uplift, the surface of load pads should be manufactured identical to the roofing profile. However, although the pads are often made of rubber or other soft elastic materials, the pads still provide an additional restraints to the roofing deformation. Therefore, the obtained roof sheeting ultimate strength or initial failure limits may be overestimated.

An experiment was conducted in this investigation to show the existence of this problem. Flat load pads were used to load the trapezoidal

type roofing sheet. In this way, the additional restraints between the roofing crests provided by loading pads were basically released. The measured wind uplift-deflection curve was plotted in Fig. 6.4 with the results obtained from the previous tests, in which the trapezoidal surface loading pads were used (see Section 4.1). In Fig. 6.4, the measured point was at the midspan of a screwed crest. It is seen that when the overall sheeting deformation was small, the roofing behaviour was similar for both flat surface loading pads and trapezoidal surface load pads. However, the limit value of equivalent pressure for the initial failure was reduced by 15% in the case of the flat surface load pads. Correspondingly, the lower and upper limit values of reaction force pre fastener for the initial failure were 820 N and 980 N, respectively. In the case of the trapezoidal surface loading pads, the limit values were 1000 N and 1160 N. Therefore, the effect of loading pad surface on the limit values for the initial failure was obvious.

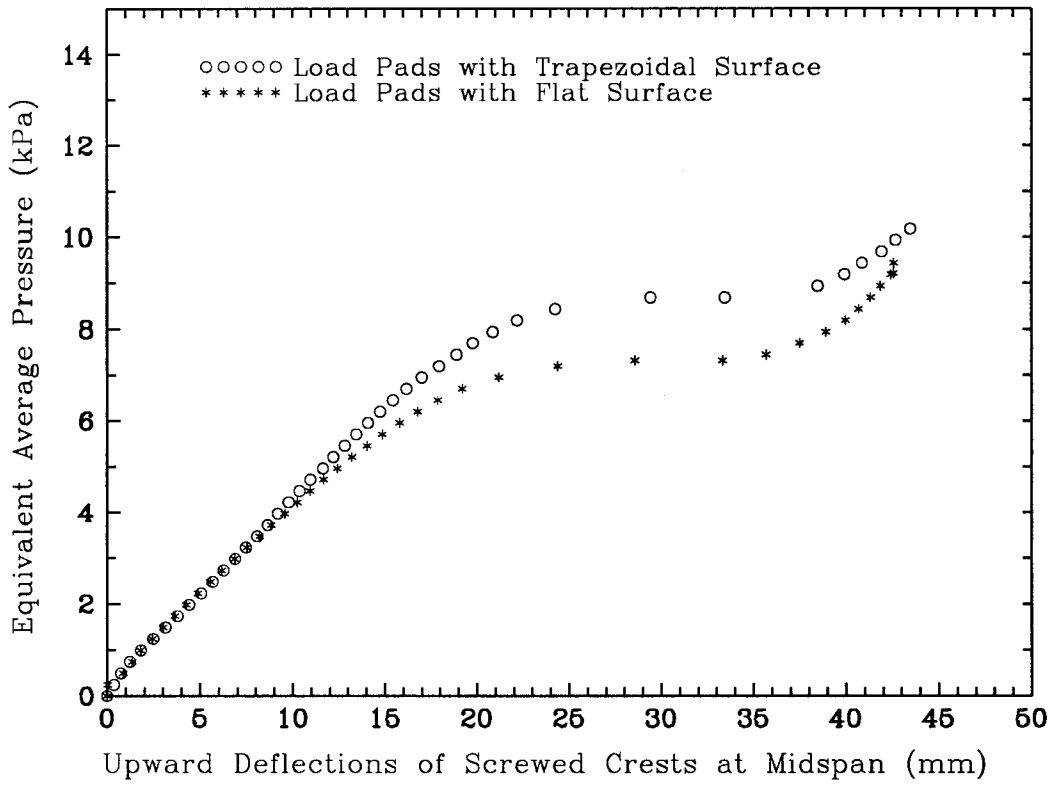

FIG.6.4 EFFECT OF LOAD PADS ON LOAD-DEFLECTION RELATION OF TRAPEZOIDAL TYPE ROOFING SHEET

Such a situation might be less serious in the arc-tangent type roofing sheet because of the smooth change of the roofing profile as well as the use of the water tube on the loading pads. The ribbed type roofing sheet has a wide pan between two crests so that the loading pad effect is expected to be

small. However, how to simulate distributed wind uplift on roofing in an easy and economical way still is a challenging subject. The application of numerical simulation, such as finite element analysis or finite strip analysis, to this field should be developed.

7. CONCLUSIONS

The main conclusions from the current investigation are as follows:

(1) The structural behaviour of light gauge steel roofing was dependent on roof sheeting profiles. For both trapezoidal and arc-tangent type roofing assemblies, the roofing sheets exhibited a large cross-sectional distortion stage (yielding stage) and a deflection hardening stage. The ribbed type roofing sheet, however, had a final failure mode of sudden fracture with cracks at bottom surface of the plastic dimple around the screw fasteners at the central support. For the roofing assembly with 900 mm equivalent span and 0.47 mm (TCT) sheeting thickness, the limit values of equivalent wind pressure for the initial failure was 5 kPa for the arc-tangent type roofing sheets and 8.5 kPa for the trapezoidal type roofing sheets. The lower and upper limit values of reaction force per fastener for the initial failure were 580 N and 650 N for the arc-tangent type roofing sheets and 1000 N and 1160 N for the trapezoidal type roofing sheets. The ultimate equivalent pressure for the ribbed type roofing sheets was 7.6 kPa while the ultimate reaction force per fastener was 1350 N.

(2) Based on the observation of large profile distortion process of the arc-tangent and trapezoidal roofing sheets, it was thought that the presence of unscrewed crests resulted in a totally different stress distribution around the screwed crests at the central support and therefore exhibited both yielding and deflection hardening stages. The wide pans rather than unscrewed crests in the ribbed type roofing made the roofing lose these two stages. It also appears from the experimental results that the shape and height of the screwed crests would affect the limit values for the initial failure and the ultimate strength of the roofing sheets.

(3) From the static testing results, it was found that the use of cyclone washers raised the initial slope of load-deflection curves, reduced the roof sheeting deflection before the initial failure, and more and less, increased the limit values of load or fastener reaction force. The fact that the use of cyclone washers was more effective for the arc-tangent type roofing sheet

than the other two types indicated a necessity of studying the shape, stiffness and size of cyclone washers relative to the shape, stiffness and size of roofing sheets.

(4) From the experimental results, it was found that for the different span roofing assemblies, the reaction force per fastener had a relatively stable limit value for the initial failure of the arc-tangent and trapezoidal type roofing sheets and for the ultimate strength of the ribbed type roofing sheet. With the increase of the roofing span, however, the allowable wind pressure still should be decreased. For the tested different span roofing assemblies, the deflection behaviour and the failure mode were in a general similarity.

(5) The increase of roof sheeting thickness resulted in a higher roof sheeting stiffness and limit value for both equivalent pressure and reaction force per fastener for the initial failure. The limited experiments also show that the thicker roofing sheets may exhibit different types of initial failure mode.

(6) As for midspan load method, the two span continuous simply supported beam assumption is reasonable in most cases. However, during the large cross-sectional distortion or large local plastic deformation, such an assumption is not satisfactory. The cyclone washer reduced local plastic deformation around the screwed fastener at the central support, and the long span roofing sometimes had a relatively small local plastic deformation so that the simple support assumption was more suitable for these cases.

(7) From the experimental results of the trapezoidal type roofing sheet loaded by flat surface loading pads, the effect of loading pad surface on the limit values of equivalent pressure or reaction force per fastener for the initial failure was considerable. An approximate 15-20% reduction of the limited values was found by using the flatted surface loading pads. Such situation might be less serious in the arc-tangent type roofing sheets because of the smooth change of the roofing profile as well as the use of the water tube. The ribbed type roofing has a wide pan between two crests so that the load pad effect is expected to be small.

8. Acknowledgments

The roofing sheets used in this project were donated by Lysaght Building Industries, to which the authors are grateful. The assistance of Mr.

D. Henderson, Mr. W. Morris and Mr. K. Abercombie in setting experiment or collecting data, and Mrs. W.J. Zhang in preparing graphs is also acknowledged.

9. References

Beck, V.R. and Stevens, L.K. (1976). " Constant repeated loading of corrugated sheeting." *Proceedings of Metal Structures Conference*, The Institution of Engineers, Australia, November, pp. 40-45.

Beck, V.R. and Stevens, L.K. (1979). " Wind loading failures of corrugated roof cladding." *Civil Engineering Transactions*, The Institution of Engineers, Australia, Vol. CE 21, No. 1, pp. 45-56.

Bushnell, D. (1985). " *Computerised buckling analysis of shells*". Martinus Nijhoff Publishers.

Ellifritt, D.S. and Burnette, R. (1990). " Pull-over strength of screws in simulated building tests." *Tenth International Specialty Conference on Cold-formed Steel Structures*, St. Louis, Missouri, U.S.A., October.

Experimental Building Station (EBS) (1978). " Guidelines for the testing and evaluation of products for cyclone prone areas." *Technical Record 440 (TR440)*, Department of Housing and Construction, Australia, February.

Gerhardt, H.J. and Kramer, C. (1986). " Wind induced loading cycle and fatigue testing of lightweight roofing fixations." *Journal of Wind Engineering and Industrial Aerodynamics*, 23, pp. 237-247.

Hancock, G. (1991). " Behaviour of purlins with screw fastened sheeting under wind uplift and downwards loading." *Postgraduate Course* - Behaviour and Design of Purlins, Sheeting and Screw-fasteners, The University of Sydney, Australia, October.

Lysaght Building Industries (1990). " *Steel roofing and walling.*" Design Manual, Sydney, Australia.

Lysaght Building Industries (1991). " *Steel roofing and walling.*" Installation Manual, Sydney, Australia.

Mahendran, M. (1988). " Static behaviour of corrugated roofing under simulated wind loading." *Technical Report* No.33, Cyclone Testing Station, James Cook University, Australia.

Mahendran, M. (1990). " Static behaviour of corrugated roofing under simulated wind loading." *Civil Engineering Transactions*, The Institution of Engineers, Australia, Vol. CE 32, No. 4, pp. 212 -218

Morgan, J.W. and Beck, V.R. (1977). " Failure of sheet-metal roofing under repeated wind loading." *Civil Engineering Transactions*, The Institution of Engineers, Australia, Vol. CE 19, No. 1, pp. 1-5.

Parsons, A.A. (1976). " Practical development from static and cyclic load testing of steel claddings." *Proceedings of Metal Structures Conference*, The Institution of Engineers, Australia, November, pp. 51-56.

Reardon, G.F. (1980). " Recommendations for the testing of roofs and walls to resist high wind forces." *Technical Report* No.5, Cyclone Testing Station, James Cook University, Australia.

Standards Association of Australia (SAA) (1991). " *Methods for tensile testing of metals.*" AS 1391 - 1991.